The interplay of soft-hard substituents in photochromic diarylethenes

Rossella Castagna[a*], Valentina Nardone[a,b], Giorgio Pariani[c], Emilio Parisini[b], Andrea Bianco[c]

[a] Dipartimento di Chimica, Materiali e Ingegneria Chimica "G. Natta", Politecnico di Milano, Piazza Leonardo da Vinci 32, 20133, Milano (Italy).

[b] Center for Nano Science and Technology @PoliMi, Istituto Italiano di Tecnologia, Via Pascoli 70/3, 20133 Milano (Italy).

[c] Istituto Nazionale di Astrofisica, Osservatorio Astronomico di Brera, via E. Bianchi 46, 23807 Merate (Italy).

Abstract

A series of diarylethene molecules with substituents of different size and chemical nature was synthesised showing that beside some intermolecular interactions involving the central diarylethene core, lateral groups clearly play a key role in the crystal packing arrangements. These structural features were further analyzed in relation to the thermal data obtained by differential scanning calorimetry (DSC) and monitored using FT-IR spectroscopy, thus providing a rationalization of the observed thermal transitions processes. The role of van der Waals interactions is crucial in driving crystal packing formation towards loosely packed arrangements characterized by large hydrophobic contact areas. Interestingly, some functional substituents favour an amorphous state after thermal treatment, a peculiar feature that can be exploited to design uniform photochromic layers.

Introduction

Progress in the development of photochromic switches requires a detailed characterization of the behaviour of photoactive compounds in the solid state. Indeed, for some applications,

completely amorphous thin films are needed, whereas for others, fully crystalline materials are required, possibly in the form of single crystals. For example, photochromic materials showing remarkable optical contrast[1,2] in specific spectral regions are attractive as active layers in photolithography, both in the form of molecules dispersed within a polymer matrix[3,4] and pure as a thin amorphous evaporated layer[5]. In the latter, the quality of the optical layer is the key to the success of the lithography process, as aggregation and crystalline domains can cause light scattering. For application of photochromic switches where crystalline materials are preferred, the long-range molecular packing order in the crystalline phase and the limited free volume for the photoconversion process may inhibit photochromic reactions. Interestingly, Irie and co-workers successfully developed thermally irreversible and fatigue-resistant photochromic crystals of furylfulgide[6] and diarylethenes[7–9].

As a result of the relative orientation of the molecules in the lattice, photochromic crystals may show specific anisotropic physical properties such as, for instance, dichroism[10,11]. Moreover, the cooperative structural changes of diarylethenes molecules that are regularly packed in a crystal may determine macroscopic mechanical modifications of the single crystal upon irradiation. In selected photochromic crystals, a change in surface morphology[12] or a dramatic shape change occurs upon light irradiation[7,13–15]. Based on this morphological behaviour, a photodriven nano-scale actuator, consisting in a rod-like crystal that bends towards the direction of the incident light, has been developed[16].

Beside twisted and bent crystals that are known to be present in nature[17], crystals that can be morphologically modified using light have been obtained[18] by exploiting the chiral properties[19–22] of photoactive molecules. These light-induced changes are caused by the shrinkage of the irradiated portion of the crystal[23] and show crystal thickness dependence[24]. This behaviour is determined by a photoisomerization gradient inside the crystal; in fact, the light-induced conversion of the photochromic layer in the solid state is

not uniform throughout the sample, and depends on both the thickness of the material and the illumination source[25]. Photochromic co-crystals[26–28] have also been studied for the development of hybridized structures of novel photonic devices. However, not only are multi-component crystals difficult to obtain, but whenever they form, energy transfer from one component to the other may prevent cyclization.

Despite the wealth of solid state diarylethene optical and photomechanical switches described to date, a large scale rational approach to the design of diarylethene molecules that takes into account the intermolecular forces governing the molecular packing in the lattice is still missing. Indeed, the effect of intermolecular interactions on the crystal packing has been stimulating an interesting and still on-going debate in the field of photochromic switches[29–35].

Here we show how the subtle interplay of substituents of different size and chemical nature affects the packing, the morphology and the aggregation of active diarylethenes in the solid state. Specifically, we have designed a series of molecules that share the same 1,2-bis-(2-methyl-5-phenyl-3-thienyl)perfluorocyclopentene central moiety, but with their phenyls differently substituted in the *para*-position (Fig. 1). We show that, beside some intermolecular interactions involving the central moiety of the diarylethenes, lateral groups play a key role in guiding and stabilizing the crystal packing arrangements. We relate the nature and the extent of the observed intermolecular interactions within each crystal to the Differential Scanning Calorimetry (DSC) profile of the corresponding molecule, thus providing a rationalization of the progression of the thermal transitions in the studied materials. Overall, extended Van der Waals interactions guide nucleation and crystal growth both from solution and from the melt, as shown by the evolution of IR spectra with time.

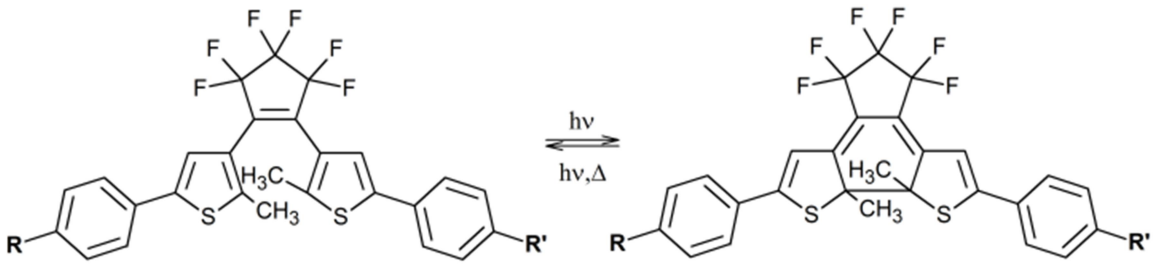

DTE-1	R = CN	R' = CN	**DTE-5**	R = CN	R' = $OC_{12}H_{25}$
DTE-2	R = CN	R' = OMe	**DTE-6**	R = OC_6H_{13}	R' = OC_6H_{13}
DTE-3	R = OMe	R' = OMe	**DTE-7**	R = $OC_{12}H_{25}$	R' = $OC_{12}H_{25}$
DTE-4	R = COOH	R' = $OC_{12}H_{25}$			

Figure 1 - Photochromic reaction in diarylethenes and chemical structure of the molecules under investigation.

Materials and Methods

All the photochromic compounds **DTE-1** to **DTE-7** were synthesized according to the procedures reported in the Supplementary Material

Crystals obtained from solution: crystals of **DTE-1** to **DTE-7** were obtained by slow solvent evaporation or by vapour diffusion, as described in detail in the Supplementary Material.

Melt derived crystals: **DTE-7** powder was heated up to 130°C at a 10°C/min rate, kept for 10 minutes at this temperature to ensure the complete melting of the powder, fast cooled to 65°C and then maintained for three hours at this temperature to perform isothermal crystallization. Then, the sample was slowly cooled down to room temperature.

^{1}H NMR spectra were collected using a Bruker ARX 400. *Mass spectroscopy* was carried out using a Bruker Esquire 3000 plus.

UV−vis absorption spectra UV-vis spectra were recorded with a Varian Cary 5000 spectrophotometer from dilute hexane solution (<10^{-5} M) and from thin film of the pure compound deposited onto quartz. The spectrophotometer was equipped with the integrating sphere (DRA2500) to measure the diffuse transmittance in the case of thin films. Starting from the open form, the photochromic reaction was triggered by illumination of the solution

or the thin film using quasi-monochromatic UV light with wavelength corresponding to the absorption maximum of the open form, until the photostationary state (PSS) was reached.

FTIR spectra were recorded using a Nicolet NEXUS FTIR interferometer (DTGS detector). In order to monitor the melting and isothermal melt crystallization process of **DTE-7**, the compound was dissolved in diethyl ether and drop-casted as a thin film on a ZnSe substrate. The substrate was then set into a variable temperature cell Linkam (THMS 600) and positioned under the objective of the IR-microscope stage. Two different thermal programs were set:

i) the specimen was heated from room temperature up to 150°C in an argon atmosphere at a 10°C/min heating rate. IR spectra were collected (256 scans, resolution 4 cm^{-1}) at different temperatures.

ii) the specimen was heated from room temperature up to 150°C in an argon atmosphere with a 20°C/min heating rate. In order to monitor the isothermal crystallization process the specimen was cooled down to the desired crystallization temperature. The temperature was kept constant following the evolution of the crystallization process. IR spectra were collected every 100 seconds with 32 scans and 4 cm^{-1} resolution.

A baseline correction was applied to all the IR spectra. In general, the area of the bands was calculated by integrating each spectrum in the desired region (keeping the spectral boundaries constant). In order to compare the different areas of the spectra during the crystallization process, normalization to the peak area at 1600 cm^{-1} was applied. All these operations were performed using OMNIC 8.0 (Thermo Electron Corporation). The Avrami model[36–38] was used to fit the FTIR data from the isothermal crystallization process. A guess of the induction time was made from the change in the position of the CH stretching peak. The initial values of A_0 and A_{max} were determined as the mean of 10 points in the minimum and maximum of the normalized FTIR area at the beginning and at the end of the crystallization process, respectively. A_0, A_{max}, k_{app}, and n were then determined by the best

fit with a least-squared method as a function of induction time, which was varied in the proximity of the guess value and used as a fixed parameter in the fitting procedure. The best induction time was then obtained as the one minimizing the fitting residuals.

DFT calculations have been performed using Gaussian 09 (G09RevD.01) with a basis set 6-31G(p,d) and B3LYP as functional. The results of the calculations are reported in the Supplementary Material.

For the *Differential Scanning Calorimetry (DSC)* analysis, the aluminium DSC pan was filled with approximately 3.5 mg of compound powder. DSC thermograms for all samples were measured with a DSC SEIKO 6300, under nitrogen. The general procedure for DSC scans consisted of a heating step from 0 to 250°C with a heating rate of 20°C/min and a cooling scan from 250°C to 0°C at a 5°C/min rate. For compound **DTE-7**, further DSC analyses were conducted by heating from 0 to 250°C and cooling back to 0°C at a scan rate of 1°C/min.

The X-ray† data for **DTE-2**, **DTE-4**, **DTE-5**. **DTE-6** and **DTE-7** were collected at 100K on a Bruker X8 Prospector APEX-II/CCD diffractometer, using CuKα radiation (λ=1.54050). All structures were solved by direct methods and refined using the SHELX-97 package[39]. All the structures were analyzed by Mercury[40], and the images were generated using PyMol[41] and Chimera[42]. The cif files of **DTE-1** and **DTE-3** were downloaded from the Cambridge Structural Database[43] (CCDC entries 652100 and 185944 respectively)

Results and discussion

1,2-Bis-(5-chloro-2-methyl-3-thienyl)perfluorocy-clopentene (**9**) was synthetized as previously reported[44]. This photochromic dichloride precursor is a versatile substrate that provides different symmetrically or asymmetrically substituted diarylethenes by Suzuki cross-coupling with either boronic acid or pinacol ester (Scheme 1).

The asymmetrically substituted **DTE-2** was synthesized by a one-pot coupling reaction, where the two boronic derivatives were sequentially introduced. Since in the symmetrically substituted dithienylethenes the coupling involving boronic derivatives bearing the cyano group led to the product in low yield, we introduced 4-cyanophenylborinic acid as a first coupling reactant in excess with respect to the 1,2-bis-(5-chloro-2-methyl-3-thienyl)perfluorocyclopentene **9**. This allowed maximization of the yield of the asymmetrical dithienylethene **DTE-2** (38%). **DTE-3** was also obtained in good yield (27%). On the contrary, despite the long reaction time, **DTE-1** was produced in a very low yield (6%). The same synthetic procedure was followed for **DTE-4**, but with a lower overall yield. The symmetrical dodecyloxy-substituted derivative **DTE-7** was also collected, while the symmetrical carboxy-substituted dithienylethene was retained in the silica column during the purification of the crude.

As an alternative method, the Suzuki-Miyaura reaction was also carried out under super-heated conditions using 1,1'-bis(di-tert-butylphosphino)ferrocene palladium dichloride ($Pd(dbpf)Cl_2$), which is a commercially available, air and water-stable catalyst. According to Moseley *et al.*[45], aryl chlorides react with sterically and electronically demanding boronic acids to give in most cases complete conversion. Here, both 4-cyanophenylboronic acid pinacol ester and 4-dodecyloxybenzene boronic acid (synthesized from 4-bromophenol, as reported in Scheme 1) the catalyst, and 1,2-bis-(5-chloro-2-methyl-3-thienyl)perfluorocyclopentene **9** were simultaneously introduced in a capped vial and heated under microwave to obtain **DTE-5**. The overall yield strongly increased (86%), with a remarkable improvement also in the formation of **DTE-1** (32%). **DTE-7** was also collected from the same reaction in good yield (28%).

DTE-6 was synthesised in 90% yield from **DTE-3** by cleavage of the methoxy group and subsequent reaction with 1-bromohexane (Scheme 1).

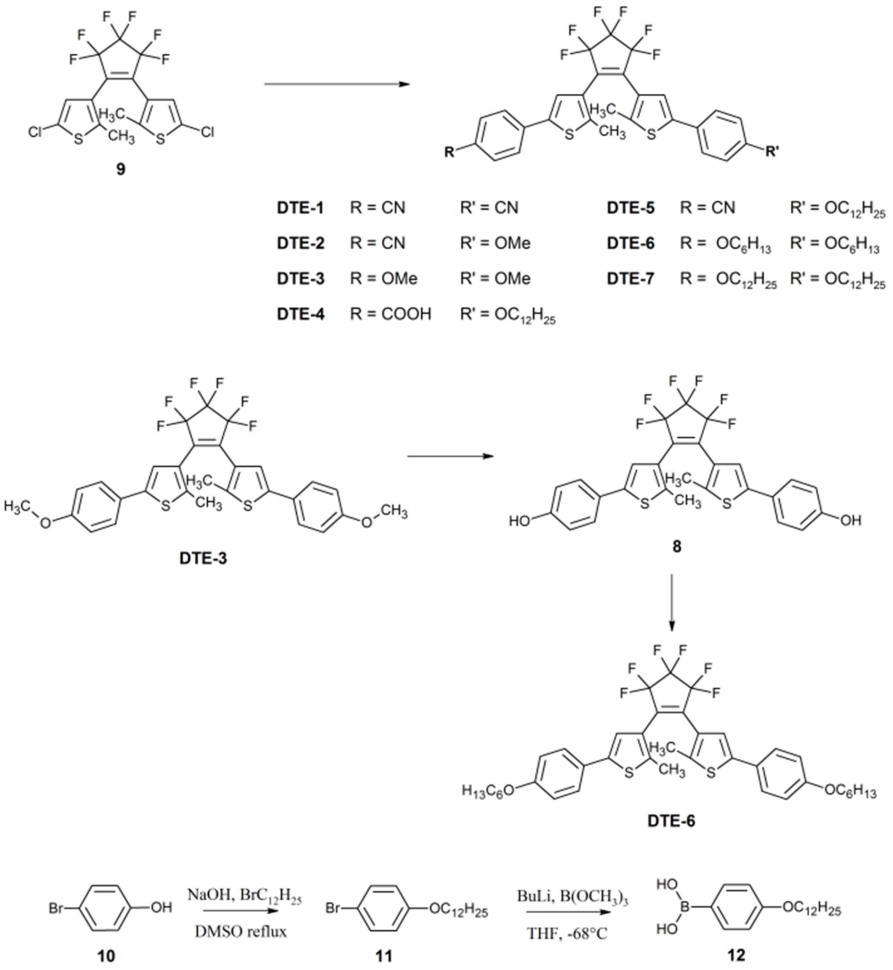

Scheme 1 - Synthetic route for DTEs under investigation

The UV-vis spectra of all the synthesized **DTE**s are reported in Fig. 2. In particular, the spectra at the photostationary state for the open and closed forms in hexane solution (solid lines) and for the closed form in thin film (dotted line). They show the typical electronic features of diarylethenes: upon irradiation with UV light, the transparent open form converts into a coloured closed form that is thermally stable. The closed form has a broad absorption band in the visible region whose position shifts in wavelength depending on the chemical structure of the molecule[2]. For all **DTE**s, photochromism occurs both in solution and in the solid state (all the UV-vis spectra in the solid state are reported in Supplementary Material Fig. S5). A remarkable broadening and a red-shift of the visible band is observed for all the compounds at the solid state in comparison to the solution. This is consistent with

the data reported in literature for films of amorphous diarylethenes, where bathochromic shifts as large as 20nm in comparison with that of the hexane solution were observed [46–48]. A similar behaviour is usually observed in high-concentration solutions, where intermolecular interactions are stronger and transitions at lower energies arise [46]. A lower conversion to the coloured form is also reported in bulk amorphous films, which may explain the differences in the absorption spectra at the PSS state below 400nm. It is also worth noting that, for non-amorphous materials, a scattering contribution is present in the spectra at the solid state and, since the scattering effect is more pronounced at shorter wavelengths, the differences between the spectra are enhanced in the UV region.

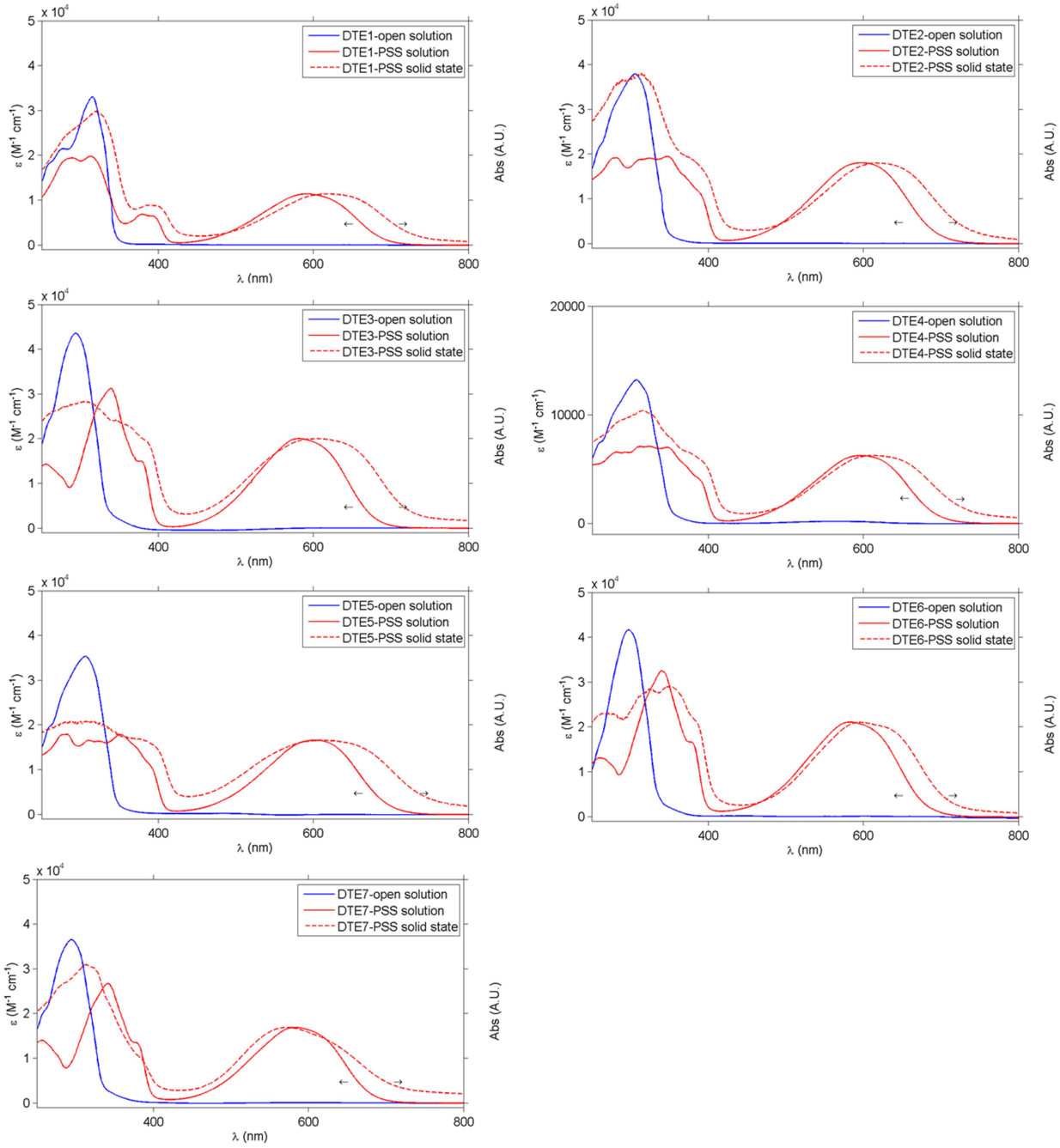

Figure 2 – UV-vis spectra of different DTEs compounds. Solid line: spectra in hexane solution in the open form (blue line) and in the PSS state (red line), scale bar on the left. Dotted line: spectra in the solid state measured on a thin film of pure compound deposited onto quartz substrate, scale bar on the right. For each compound both in solution and in the solid state the spectra of the closed form are reported at the photostationary state conversion (PSS), obtained by illumination of the sample at the absorption peak of the open form.

Absorption maxima of the **DTE** in hexane solution with the corresponding absorption coefficients are summarized in Table S3. All the **DTE**s studied herein that bear withdrawing groups (i.e. **DTE-1**, **DTE-2**, **DTE-4** and **DTE-5**) show red-shifted absorption bands, both in the open and in the closed form. This is due to the more extended conjugation provided by

the CN triple bond or the C=O double bond. Moreover, a decrease in the molar extinction coefficient (ε) is registered for the diarylethenes substituted with electron-withdrawing groups. In the closed form, the asymmetrically substituted dithienylethenes (i.e. **DTE-2**, **DTE-4** and **DTE-5**) have the actinic bands in the visible range located at lower energies (i.e. 597, 597 and 603 nm, respectively) as the push-pull effect adds to the extension of the conjugation system. The symmetrically donor substituted **DTE** (i.e. **DTE-3**, **DTE-6** and **DTE-7**) show very small differences in the absorption maxima, thus indicating that the length of the alkyl chain has a negligible effect in solution.

Crystal structures

In solution, open form-dithienylethenes exist as an equilibrium of two conformational isomers, one with anti-parallel C_2 and the other with parallel C_s symmetry, only the former being photoactive. In the solid state, all the compounds described herein feature two thiophene rings that are out-of-plane with respect to the ethene bridge and an *anti*-parallel conformation of the substituents. Moreover, in all the reported structures the distance between the reactive carbons is shorter than 4.2Å (details in the Supplementary Material Table S4), which is a fundamental requirement for the maintenance of photochromism in crystals[49]. These two elements are consistent with the evidence that all the **DTE** crystals described herein are photochromic.

The crystal packing arrangement of the molecules is strongly influenced by the size and the nature of the substituents introduced. The cyano-cyano substituted **DTE-1**[50], the asymmetrical substituted **DTE-2** and two of the four available polymorphs of the methoxy-methoxy substituted **DTE-3**[51], which all bear small substituents, show a very similar packing arrangement. The packing arrangement of **DTE-2** is shown in Fig. 3. At the two ends of the molecule, the relative orientation of the thiophene and the benzene rings is essentially identical (the torsion angle of the benzonitrile and the methoxybenzene moieties

with respect to their corresponding thiophenes is -18.08° and 20.22°, respectively). In the lattice, next-neighbouring molecules form an anti-parallel packing arrangement stabilized by an S-π interaction between the sulfur at the cyanophenyl end of the molecule and the phenyl ring of the benzonitrile moiety of the partner molecule (the angle is 84.69° and the distance 3.64Å). Conversely, the other thiophene ring of the reference molecule and the methoxy-substituted ring of the interacting molecule are almost parallel (18.48°), featuring a centroid-centroid distance of 3.91Å. and a S-centroid distance of 3.24Å. Moreover, a stabilizing π-π interaction is established between two benzonitrile rings from two molecules belonging to two different dimers (the distance between the two centroids is 4.15Å).

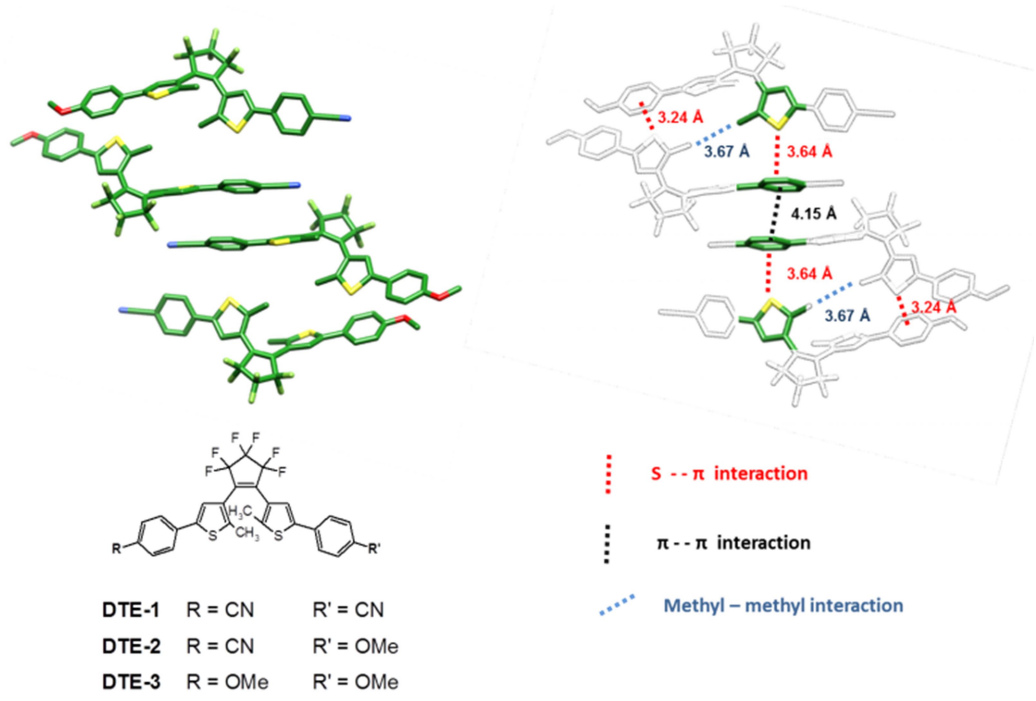

Figure 3 - Crystal packing of DTE-2 (on the left), and highlight of the stabilizing interactions described in the text (on the right). A very similar packing arrangement is also found for DTE-1 and DTE-3, not shown here.

In **DTE-5**, the methoxy group of **DTE-2** is replaced by a long (C_{12}) alkoxy chain. The alkoxy chains of two next neighbouring molecules are essentially parallel and form Van der Waals contacts (4.1-4.5Å) along their entire extended conformation. Driven by this interaction, a stacking arrangement of the molecules is formed along the *b* axis of the **DTE-**

5 unit cell, resulting in an antiparallel interdigitation of the long aliphatic chains, a feature that is also shared by the **DTE-7** structure presented herein (see Fig. S2 in the Supplementary Material).

In the **DTE-5** crystal, like in **DTE-2**, within the pair of more closely interacting molecules the thiophene ring of the first molecule is almost perpendicular to the benzonitrile ring of the next-neighbouring molecules (84.47°, with a sulphur-benzene distance of 3.64Å) and, at the alkoxy-substituted end of the dithienylethene, the thiophene and the benzene of the two next neighbouring molecules are almost parallel (17.68°, with a 4.50Å distance between the centroids).

In **DTE-4** intermolecular hydrogen bonding involving the carboxylic acid moiety at one end of the molecule drives the packing arrangement, where head-to-head dimers are formed in the crystal (2.64Å). An electrostatic interaction between the thiophene S atom and the carboxylic group of the next nighboring molecule (3.31Å) further stabilizes the observed conformation (Fig. 4).

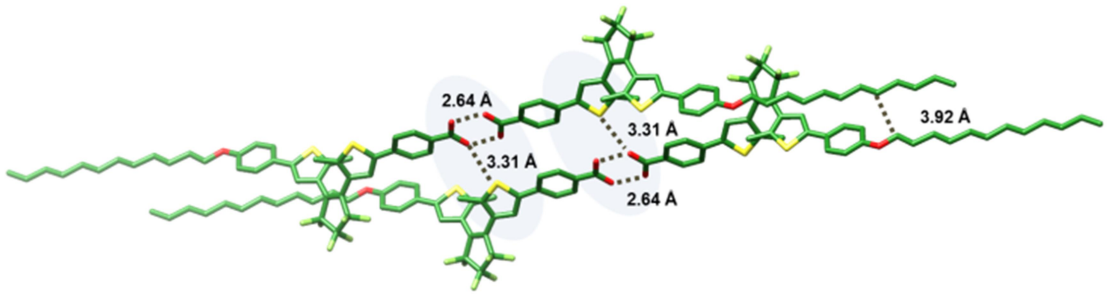

Figure 4 - Crystal packing of DTE-4 in a head-to-head dimer conformation with a bidentate hydrogen bonding between the carboxylic acid, electrostatic interaction between the thiophene S atom and the carboxylic acid and hydrophobic contacts between the alkyl chains.

Compounds **DTE-3**, **DTE-6** and **DTE-7** are all symmetrically substituted, and carry an alkoxy-benzene moiety of different length (C_1, C_6, and C_{12}, respectively). **DTE-6** crystallizes with half a molecule in the asymmetric unit and the torsion angle between the

thiophene ring and the benzene ring is -14.88°. Within the pair formed by the two more closely interacting molecules in the **DTE-6** crystal, S-π interactions are present, where the thiophene ring of one molecule is almost perpendicular to the centroid of the benzene ring of the partner molecule, with a distance of 3.87Å. In the **DTE-6** crystal, the alkoxy chains show structural disorder. Although two well-defined alternative conformations of the alkoxy chains could be clearly seen and accounted for in the final model, the relatively large thermal parameters of the atoms suggest a certain degree of residual dynamic disorder in the molecule even if the data were collected at low temperature. This is in agreement with the disorder observed in two polymorphs of the same molecule that were previously obtained with a different crystallization solvent (acetone) at room temperature[52].

Interestingly, the crystal structure of **DTE-7** shows very different torsional angles between the thiophene rings and the benzene rings at the two ends of the molecule, namely 32.47° on one side and completely planar on the other side (2.31°). The long aliphatic chains of **DTE-7** account for a large portion of the molecule, and the packing arrangement is guided by the optimization of the number and extent of van der Waals contacts between these long hydrophobic substituents. Each **DTE-7** molecule makes two distinct sets of short C-C contacts (in the range of 4.2-4.5Å) with the next neighbouring molecules in the lattice (Fig. 5), forming a packing arrangement that extends indefinitely and accounts for all the stabilizing interactions in the crystal. These hydrophobic interactions lead to the formation of an interdigitated arrangement of the chains similar to that observed for the alkyl moieties of **DTE-5**. Interestingly, alkyl chain interdigitation is not observed in **DTE-4**, where a hard substituent such as the carboxy group strongly dominates the crystal packing arrangement, even in the presence of a long alkoxy chain. In **DTE-7**, short intermolecular S-π interactions involving the aromatic rings connect next-neighbouring molecules to form an extended network spanning throughout the crystal. A further stabilizing intermolecular interaction

occurs between a sulphur atom of one molecule and the thiophene ring of the next-neighbouring molecule, with a S-centroid distance of 4.11Å.

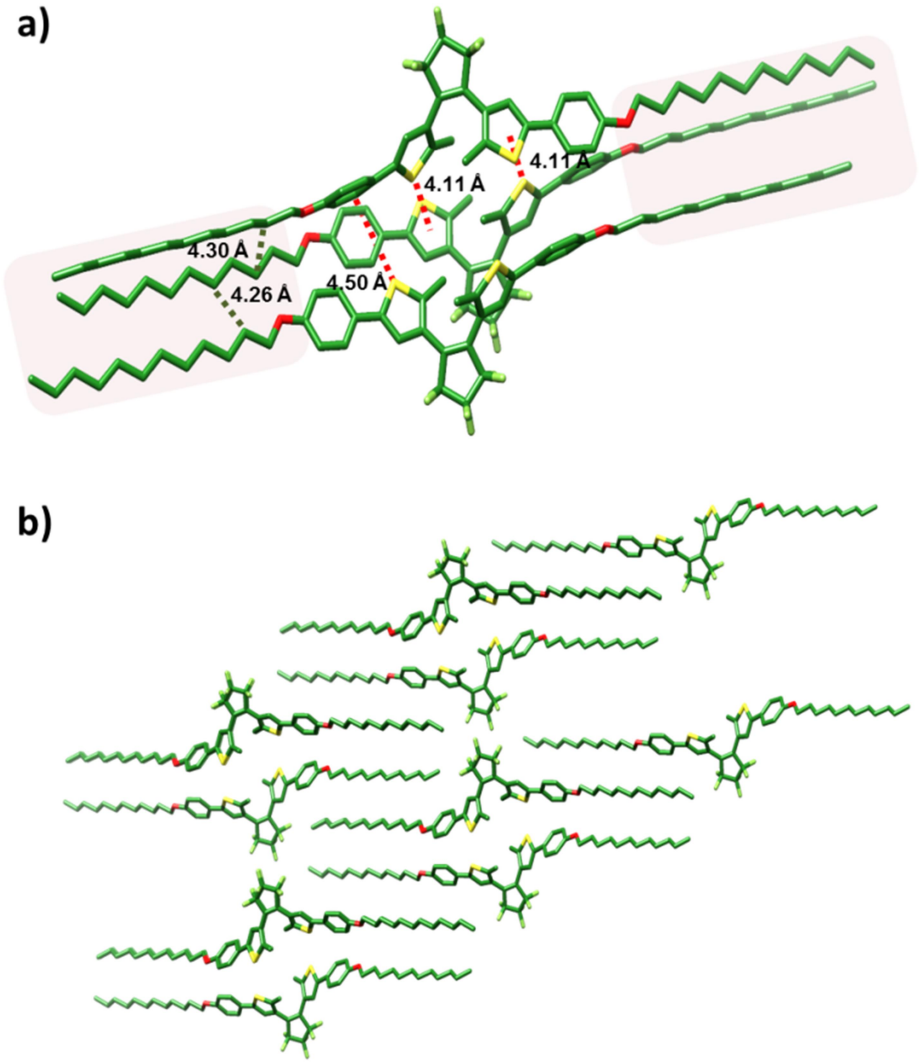

Figure 5 - (a) Crystal packing of DTE-7 highlighting the main intermolecular interactions described in the text. (b) Chain interdigitation.

Although stabilizing S-π contacts are seen in all the structures described herein, the longest S-π distance is observed in **DTE-7**, where the major stabilization energy to the packing is provided by the contacts between the long hydrophobic chains.

A general decrease in the calculated crystal density in going from **DTE-1** to **DTE-7** (Table 1) highlights the increasing contribution of the relatively weak van der Waals contacts

between the long aliphatic chains with respect to the more directional interactions that hold the shorter molecules together in the lattice. The only notable exception is **DTE-6**, where the observed conformational disorder highlights the lack of well-defined structural constraints on the short (C_6) alkoxy chains. Here, the intermolecular packing arrangement is mostly driven by the interactions between the central moieties of the molecules, resulting in the relatively high calculated crystal density for this compound (Table 1).

Thermal behavior

Differential Scanning Calorimetry (DSC) analysis was performed in order to study the possible occurrence of thermal transitions and to provide information on the solid phase. DSC scans are reported in the Fig. S6 of the Supplementary Material, while the melting temperatures of the DTEs are summarized in Table 1. The melting temperatures of all the DTEs studied herein are remarkably different, going from 90°C to 216°C; moreover, they do not relate to the differences in molecular weight among the members of the series. Rather, the melting temperature values are consistent with the diverse sets of stabilization interactions that these different molecules form in the solid state. Indeed, interactions between neighbouring molecules in the crystal explain why molecules bearing the smallest side groups (**DTE-1**, **DTE-2** and **DTE-3**) show melting temperatures higher than those of species with one or two alkyl chains (as for **DTE-5**, **DTE-6** and **DTE-7**). Interestingly, in the **DTE-1** packing arrangement, the nitrile groups form a π-π interaction with the benzene rings of adjacent molecules; these contacts provide further stabilization energy, which likely accounts for the sharp increase in density and melting temperature of this compound with respect to **DTE-2** and **DTE-3**, whose packing arrangements are otherwise very similar. In the case of **DTE-3**, **DTE-6** and **DTE-7**, the longer the alkyl chains the lower the melting temperature. Moreover, crystal stability appears to be higher (e.g. higher melting temperature) when only one long alkyl chain is present instead of two (see **DTE-5** with

respect to **DTE-7**). In the case of **DTE-4**, the presence of one long alkyl chain is counterbalanced by the strong, stabilizing bidentate hydrogen bonding interaction between carboxyl groups.

Table 1 - Melting temperature and crystal density of different diarylethene crystals obtained from solution measured with DSC.

Diarylethene	Melting temperature (°C)	Density g/cm^3
DTE-1	216	1.526
DTE-2	170	1.514
DTE-3	147	1.451
DTE-4	147	1.354
DTE-5	130	1.356
DTE-6	120	1.380
DTE-7	90	1.220

It is worth noting that the presence and the length of the alkyl chains as well as the melting temperature of the different crystals show a good correlation with the calculated crystal densities. The highest density, and therefore the most efficient packing, is found for **DTE-1**, followed by **DTE-2** and **DTE-3**. Notably, **DTE-2** and **DTE-3** are characterized by a virtually identical packing arrangement. In the alkyl-substituted compounds, crystal densities are smaller, likely due to the increased size and more elongated shape of the molecules. Within the molecules carrying the long (C12) alkoxy chain, the packing arrangement of **DTE-4** and **DTE-5**, which are both asymmetric as they also carry a short substituent (COOH and CN, respectively), have similar density, while the symmetrically-substituted **DTE-7** is more loosely packed..

As for **DTE-7**, this is the only photochromic compound showing a crystallization transition peak during the DSC cooling scan from the melt phase. In fact, an endothermic peak is recorded at 50°C during the DSC scan (from 250°C to 0°C at 1°C/min cooling rate). At an initial visual inspection, melt-derived **DTE-7** single crystals obtained from isothermal crystallization show exactly the same crystal habit as those obtained from solution. The X-ray diffraction analysis of several crystals from the same batch always provided the same

unit cell parameters as those of the crystal obtained by evaporation, indicating that recrystallization from the melt affords the same **DTE-7** crystal form. The peculiar behaviour of **DTE-7** suggests that the presence of two long alkoxy chains (C12) facilitates crystal formation from the melt phase. To investigate such behaviour, both the melting and the crystallization process were followed stepwise by IR spectroscopy.

Role of soft substituents

The FT-IR spectra of **DTE-7** at room temperature (25°C) and after the melting process (at 150°C) are reported in Fig.6. The spectrum interpretation was obtained by the normal mode analysis performed with the DFT calculations.

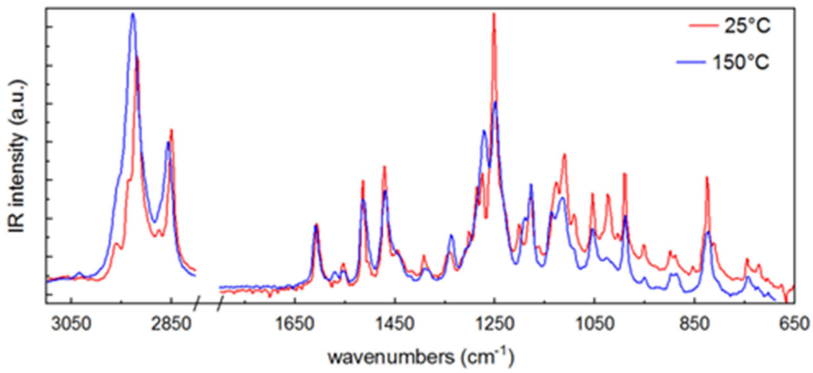

Figure 6 – FT-IR of a DTE-7 in the solid state at 25°C (red) and in the melt state at 150°C (blue).

A shift of both the asymmetric and symmetric stretching bands during the melting process is clearly visible in the C-H stretching region (3000-2700 cm^{-1}), which is consistent with the data reported in the literature for alkyl chains in liquid and crystalline phases (see for example[53]). At the same time, a broadening of the same bands occurs, causing the loss of the band structure. A backward shift to shorter wavenumbers is reported for the cooling process.

In the fingerprint region, the spectra are dominated by bands related to the normal modes of the perfluorocyclopentene and to the bending vibrations of the aliphatic chains (1350-1200 cm^{-1}). The presence of $–CH_2-$ rocking at 720 cm^{-1} (which is active only for long methylene

chains) and bands in the CC stretching region (1020 cm^{-1}) supports the occurrence of an intramolecular order of the lateral chains.

During the melting process, large changes occur in the 1350-1200 cm^{-1} region, consisting in *i)* the destructuration of the bands at 1280 and 1290 cm^{-1} and *ii)* the increase of the intensity ratio between the bands at 1280/1290 cm^{-1} and the band at 1240 cm^{-1}. These bands refer to normal modes that involve the C-F stretching of the perfluorocyclopentene and the methylene wagging of the lateral chains. This finding is consistent with the decrease of long-range order in the sample as melting occurs. In the process, the coupling of the two modes changes, thus resulting in wider bands. Another evidence of the increase in chain disorder comes from the rocking band at about 720 cm^{-1}. This band, which is very weak in the melted form, becomes stronger in the crystalline form thanks to the increase of long-range order.

A clear fingerprint of the crystalline state is the band at 1023 cm^{-1} that lies in the CC and CO region. The band is clearly evident in the crystalline phase (obtained both from solution and by cooling of the melt) while it disappears in the melt. According to the DFT calculations, this normal mode originates from a combination of CC stretching, partially involving the CO stretching (see figure S7 in the Supplementary material).

Isothermal crystallization mechanism

To elucidate the contributions of the different moieties to the crystal packing, the melting and the isothermal crystallization of **DTE-7** were monitored by FT-IR spectroscopy during isothermal crystallization at 60°C and 65°C. The intensity of the CH stretching bands shows no phase dependence, as previously reported.[54] Although the total intensity does not vary, both the asymmetric and symmetric CH stretching wavenumbers shift while the melt converts to the crystal phase. The evolution of the peaks position during the crystallization process is reported in Fig. 7.

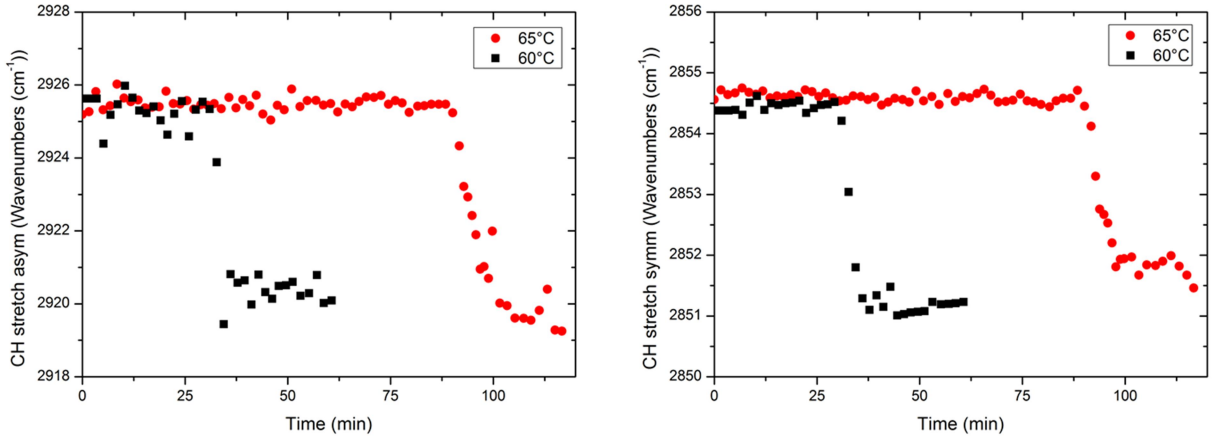

Figure 7 - Peak position of the asymmetrical CH stretching of DTE-7 (left) and the symmetrical CH stretching (right) as a function of time during isothermal crystallization at 60 °C and 65 °C.

As expected, bands shift towards shorter wavenumbers as the transition from melt to crystal occurs. The starting time of the isothermal crystallization depends on the temperature, that is the lower the temperature the shorter the starting time. Given a certain temperature of isothermal crystallization, both symmetrical and asymmetrical CH stretching modes show the same transition time.

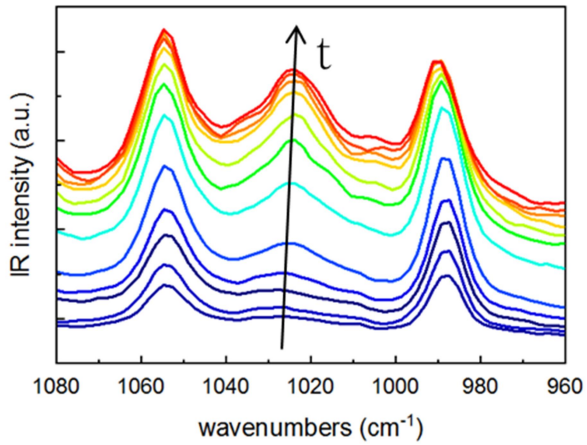

Figure 8 - A detail of the FT-IR of DTE-7 in the C-C stretching partially involving the C-O stretching region during iso-thermal crystallization at 60°C.

The same transition appears when monitoring the evolution of the infrared band at 1023 cm^{-1} (Fig. 8), which, according to DFT calculations (see figure S7 in the Supplementary material), is sensitive to the regularity of the alkoxy lateral chains, i.e. the more transplanar the lateral chain the higher the band intensity. Hence, it is possible to follow the intensity evolution of the band at 1023 cm^{-1} as a marker of the degree of crystallinity of the sample. Accordingly, the crystallinity fraction (Xc) can be calculated from the area of the marker band, as follows:

$$X_C = \frac{A_t - A_0}{A_{max} - A_0}$$

where A_t is the band intensity during isothermal crystallization at the time t, A_0 is the intensity at the beginning of the isothermal crystallization and A_{max} is the intensity at the end of the process.

The crystallization fraction obtained from the normalized area of the band at 1023 cm^{-1} is reported in Fig. 9 as a function of the crystallization time for isothermal cooling at 60°C and 65°C. In passing from the melt to the solid state, an increase of the infrared intensity is evident when following the isothermal crystallization process at both temperatures. Moreover, there is a correlation between the shift in the position of the CH stretching band and the evolution of the intensity of the 1023 cm^{-1} band. Referring to the same temperature, the two transitions start at the same time and have a similar duration, as can be evidenced by comparing Fig. 7 and Fig. 9. We conclude that the two phenomena can be ascribed to the same physical transition and are both markers of the crystallization process.

The kinetics of the isothermal crystallization of polymers[55–57], small molecules[58,59] and alloys[60] is described by means of the Avrami or modified Avrami model. The former is used for the evolution of the crystallization process under isothermal conditions, while the latter applies to non-isothermal processes[54]. Since we have performed an isothermal

cooling and monitored the evolution of the target band at 1023 cm^{-1}, we apply the standard Avrami model, as follows:

$$X_c = \frac{A_t - A_0}{A_{max} - A_0} = 1 - e^{-k(t-t_0)^n}$$

where k is the crystallization rate constant, which depends on the nucleation and growth rates, t is the time of the crystallization, t_0 is the induction time, and n is the Avrami exponent. The exponent value is related to the nature of the nucleation and to the geometry of the growing crystals, namely: n=4 volume nucleation and three dimensional growth, n=3 volume nucleation and two dimensional growth, n=2 volume nucleation and one dimensional growth, n=1 surface nucleation and one dimensional growth[60].

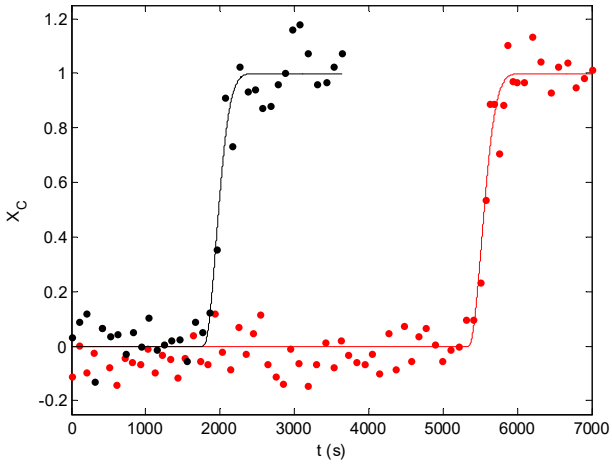

Figure 9 - Evolution of the crystallization fraction of DTE-7 obtained from the FT-IR normalized area of the 1023 cm-1 band for isothermal crystallization at 60°C (black dots) and 65°C (red dots). The solid line represents the Avrami fitting at each temperature.

The X_c experimental data are fitted according to the model and the best fitting parameters are reported in Table 2. The Avrami fittings are reported in Fig. 9 for both crystallization temperatures. As expected, the induction time is shorter for the crystallization at 60°C.

On the other hand, the difference in the intensity ΔA increases with the temperature, since a slower crystallization process leads to a higher degree of crystallinity. Moreover, according to the model, the best fit occurs for a value of n close to 2, which means that the crystallization starts from a heterogeneously nucleated sample and follows a one-dimensional growth of the crystals confined in a thin layer. Therefore, crystals grow from different nucleation seeds and enlarge as lamellae of constant thickness until all the material has transitioned to the solid state.

Table 2 - Best Avrami fitting parameters for isothermal crystallization at 60°C and 65°C.

	60°C	**65°C**
k_{app} (s^{-n})	(1.9± 0.3) x 10^{-5}	(1.9± 0.2) x 10^{-5}
t_0 (s)	1780 ± 20	5345 ± 20
N	2.0 ± 0.3	2.0 ± 0.2
A_{max}	0.290 ± 0.001	0.400 ± 0.001
A_0	0.095 ± 0.006	0.178 ± 0.007
$\mathbf{\Delta A = A_{max} - A_0}$	0.195	0.222

Conclusions

Although in 1,2-dithienylethenes electroactive substituents are usually introduced to tune the electronic transitions (i.e. color) of the molecule, their role in affecting the molecular aggregation or regular packing mode in the solid state cannot be neglected. In all the crystal structures reported herein, the stabilization energy in the lattice is provided by intermolecular interactions involving both the diarylethene core and the lateral substituents. This is particularly evident when side groups that induce hard interactions, such as for instance carboxylic acid, are present. However, soft lateral groups providing weak Van der Waals interactions between molecules can also have a strong influence on the crystal packing when they are extended over long alkyl chains. Here, we showed that different substituents dramatically affect the intermolecular packing arrangement in the crystals, likely driving the nucleation and crystallization process. We have demonstrated that the extent and the nature of the interactions they form in the crystals correlate well with the melting temperatures of the

compounds. Moreover, we have shown the unique role of long alkyl chains (**DTE-7**) in inducing re-crystallization from the melt state in a 3D-zipper fashion. Relatively to all the other compounds of the series, the unique ability of **DTE-7** to re-crystallize from the melt suggests the existence of a threshold, determined by the number and the length of the alkyl chains, above which they are sufficiently strong to drive the molecular recognition process and assembly at the crystalline state both from solution and from the melt. Moreover, by correlating FT-IR spectroscopy data with DFT calculations, the crystallization process of the diarylethene substituted with two long alkyl chains (**DTE-7**) has been followed over time and rationalized. Finally, the application of the Avrami model suggests that the nucleation process results in the one dimensional linear growth of a thin lamella.

Acknowledgements

The European Union ("Marie Curie" FP7 IRG grant DETACH to E.P. and OPTICON project, FP7 to A.B. and C.B.) is gratefully acknowledged for financial support.
The authors thank L. Brambilla for help with FT-IR spectra measurements and A. Cristina for graphical support.

Notes and References

† Ccdc: 1016933-1016937 contain the supplementary crystallo-graphic data for this paper. These data can be obtained free of charge from the Cambridge crystallographic data center via www.ccdc.cam.ac.uk/data_request/cif. Electronic Supplementary Material available: [Synthetic procedure, DFT calculation, crystal data, UV-vis spectra and DSC traces]. See DOI: 10.1039/b000000x/

Corresponding Author

* Rossella Castagna – rossella.castagna@polimi.it

[1] C. Bertarelli, A. Bianco, R. Castagna, G. Pariani, Photochromism into optics: Opportunities to develop light-triggered optical elements, J. Photochem. Photobiol. C Photochem. Rev. 12 (2011) 106–125. doi:10.1016/j.jphotochemrev.2011.05.003.

[2] M. Irie, Diarylethenes for Memories and Switches., Chem. Rev. 100 (2000) 1685–1716. http://www.ncbi.nlm.nih.gov/pubmed/11777416.

[3] T.L. Andrew, H.-Y. Tsai, R. Menon, Confining light to deep subwavelength dimensions to enable optical nanopatterning., Science. 324 (2009) 917–21. doi:10.1126/science.1167704.

[4] G. Pariani, R. Castagna, R. Menon, C. Bertarelli, A. Bianco, Modeling absorbance-modulation optical lithography in photochromic films, Opt. Lett. 38 (2013) 3024–3027. doi:10.1364/OL.38.003024.

[5] P. Cantu, N. Brimhall, T.L. Andrew, R. Castagna, C. Bertarelli, R. Menon, Subwavelength nanopatterning of photochromic diarylethene films, Appl. Phys. Lett. 100 (2012) 183103. doi:10.1063/1.4710547.

[6] S. Kobatake, M. Irie, Photochromism of Furylfulgide in a Single-crystalline Phase, Chem. Lett. 33 (2004) 904–905.

[7] M. Irie, Photochromism of diarylethene single molecules and single crystals, Photochem. Photobiol. Sci. 9 (2010) 1535. doi:10.1039/C0PP00251H.

[8] T. Fukaminato, S. Kobatake, T. Kawai, M. Irie, Three-dimensional erasable optical memory using a

photochromic diarylethene single crystal as the recording medium, Proc. Japan Acad. 77 (2001) 30–35.

[9] S. Yamamoto, K. Matsuda, M. Irie, Photochromism of diarylethenes linked by hydrogen bonds in the single-crystalline phase., Chemistry. 9 (2003) 4878–86. doi:10.1002/chem.200304947.

[10] S. Kobatake, M. Irie, Single-Crystalline Photochromism of Diarylethenes, Bull. Chem. Soc. Jpn. 77 (2004) 195–210.

[11] K. Shibata, K. Muto, S. Kobatake, M. Irie, Photocyclization/Cycloreversion Quantum Yields of Diarylethenes in Single Crystals, J. Phys. Chem. A. 106 (2002) 209–214. doi:10.1021/jp0115648.

[12] M. Irie, S. Kobatake, M. Horichi, Reversible surface morphology changes of a photochromic diarylethene single crystal by photoirradiation., Science. 291 (2001) 1769–72. doi:10.1126/science.291.5509.1769.

[13] S. Kobatake, S. Takami, H. Muto, T. Ishikawa, M. Irie, Rapid and reversible shape changes of molecular crystals on photoirradiation., Nature. 446 (2007) 778–81. doi:10.1038/nature05669.

[14] M. Morimoto, S. Kobatake, M. Irie, Crystal engineering of photochromic diarylethene single crystals., Chem. Rec. 4 (2004) 23–38. doi:10.1002/tcr.10078.

[15] S. Kobatake, H. Hasegawa, K. Miyamura, High-Convertible Photochromism of a Diarylethene Single Crystal Accompanying the Crystal Shape Deformation, Cryst. Growth Des. 11 (2011) 1223–1229. doi:10.1021/cg101448m.

[16] M. Morimoto, M. Irie, A diarylethene cocrystal that converts light into mechanical work., J. Am. Chem. Soc. 132 (2010) 14172–8. doi:10.1021/ja105356w.

[17] A.G. Shtukenberg, Y.O. Punin, A. Gujral, B. Kahr, Growth actuated bending and twisting of single crystals., Angew. Chem. Int. Ed. Engl. 53 (2014) 672–99. doi:10.1002/anie.201301223.

[18] D. Kitagawa, H. Nishi, S. Kobatake, Photoinduced Twisting of a Photochromic Diarylethene Crystal, Angew. Chemie Int. Ed. 52 (2013) 9320–9322. doi:10.1002/anie.201304670.

[19] S. Yamamoto, K. Matsuda, M. Irie, Absolute asymmetric photocyclization of a photochromic diarylethene derivative in single crystals., Angew. Chem. Int. Ed. Engl. 42 (2003) 1636–9. doi:10.1002/anie.200250417.

[20] S. Yamamoto, K. Matsuda, M. Irie, Diastereoselective cyclization in chiral diarylethene crystals: polymorphism and selectivity., Org. Lett. 5 (2003) 1769–72. doi:10.1021/ol034440h.

[21] K. Uchida, S. Sukata, Y. Matsuzawa, M. Akazawa, J.J.D. de Jong, N. Katsonis, et al., Photoresponsive rolling and bending of thin crystals of chiral diarylethenes, Chem. Commun. (2008) 326. doi:10.1039/b715251e.

[22] T. Ichikawa, M. Morimoto, M. Irie, Asymmetric photoreaction of a diarylethene in hydrogen-bonded cocrystals with chiral molecules., Photochem. Photobiol. Sci. 13 (2014) 199–204. doi:10.1039/c3pp50239b.

[23] F. Terao, M. Morimoto, M. Irie, Light-driven molecular-crystal actuators: rapid and reversible bending of rodlike mixed crystals of diarylethene derivatives., Angew. Chem. Int. Ed. Engl. 51 (2012) 901–4. doi:10.1002/anie.201105585.

[24] D. Kitagawa, S. Kobatake, Crystal Thickness Dependance of Photoinduced Crystal Bending of 1,2-Bis(2-methyl-5-(4-(1-naphthoyloxymethyl)phenyl)-3-thienyl)perfluorocyclopentene, J. Phys. Chem. C. 117 (2013) 20887–20892.

[25] G. Pariani, A. Bianco, R. Castagna, C. Bertarelli, Kinetics of photochromic conversion at the solid state: quantum yield of dithienylethene-based films., J. Phys. Chem. A. 115 (2011) 12184–93. doi:10.1021/jp207210p.

[26] T. Yamada, S. Kobatake, M. Irie, Single-Crystalline Photochromism of Diarylethene Mixtures, Bull. Chem. Soc. Jpn. 75 (2002) 167–173.

[27] M. Morimoto, S. Kobatake, M. Irie, Photochromism of diarylethenes in nanolayers of a single crystal, Photochem. Photobiol. Sci. 2 (2003) 1088–1094. doi:10.1039/b307999f.

[28] M. Morimoto, S. Kobatake, M. Irie, Multicolor photochromism of two- and three-component diarylethene crystals., J. Am. Chem. Soc. 125 (2003) 11080–7. doi:10.1021/ja035277o.

[29] S. Yagai, T. Nakajima, K. Kishikawa, S. Kohmoto, T. Karatsu, A. Kitamura, Hierarchical organization of photoresponsive hydrogen-bonded rosettes., J. Am. Chem. Soc. 127 (2005) 11134–9. doi:10.1021/ja052645a.

[30] V.A. Barachevskii, R.E. Karpov, Photonics of nanostructured systems based on photochromic spiro compounds, High Energy Chem. 41 (2007) 188–199. doi:10.1134/S001814390703006X.

[31] A. Miyata, Y. Unuma, Y. Higashigaki, Aggregates in LB of spiropyrans having hydroxyl group, Bull. Chem. Soc. Jpn. 64 (1991) 1719–1725.

[32] A. V. Metelitsa, C. Coudret, J.C. Micheau, N. a. Voloshin, Quantitative investigations of thermal and photoinduced J- and H-aggregation of hydrophobic spirooxazines in binary solvent through UV/vis spectroscopy, RSC Adv. 4 (2014) 20974. doi:10.1039/c4ra02587c.

[33] N. Matsui, T. Tsujioka, Carrier mobility of photochromic diarylethene amorphous films, Org. Electron. 15 (2014) 2264–2269. doi:10.1016/j.orgel.2014.06.032.

[34] N. Katsonis, A. Minoia, T. Kudernac, T. Mutai, H. Xu, H. Uji-I, et al., Locking of helicity and shape complementarity in diarylethene dimers on graphite., J. Am. Chem. Soc. 130 (2008) 386–7. doi:10.1021/ja075917d.

[35] M. Frigoli, C. Welch, G.H. Mehl, Design of Mesomorphic Diarylethene-Based Photochromes, J. Am. Chem. Soc. 126 (2004) 15382–15383.

[36] M. Avrami, Kinetics of Phase Change. I General Theory, J. Chem. Phys. 7 (1939) 1103.

[37] M. Avrami, Kinetics of Phase Change. II Transformation-Time Relations for Random Distribution of Nuclei, J. Chem. Phys. 8 (1940) 212.

[38] M. Fanfoni, M. Tomellini, The Johnson-Mehl-Avrami-Kolmogorov model: A brief review, Nuovo Cim. 20 (1998) 1171–1182.

[39] G.M. Sheldrick, A short history of SHELX, Acta Cryst. A64 (2008) 112–122.

[40] C.F. Macrae, I.J. Bruno, J.A. Chisholm, P.R. Edgington, P. McCabe, E. Pidcock, et al., Mercury CSD 2.0 - New Features for the visualization and Investigation of Crystal Structures, J. Appl. Cryst. 41 (2008) 466–470.

[41] Www.pymol.org, PyMOL, (n.d.).

[42] E. Pettersen, T. Goddard, C. Huang, G. Couch, D. Greenblatt, E. Meng, et al., UCSF Chimera a visualization system for exploratory research and analysis, J. Comput. Chem. 25 (2004) 1605–1612.

[43] F.H. Allen, The Cambridge Structural Data-base: a quarter of a million crystal structures and rising, Acta Crystallogr. B58 (2002) 380–388.

[44] S. Hermes, G. Dassa, G. Toso, A. Bianco, C. Bertarelli, G. Zerbi, New fast synthesis route for symmetric and asymmetric phenyl-substituted photochromic dithienylethenes bearing functional groups such as alcohols, carboxylic acids, or amines, Tetrahedron Lett. 50 (2009) 1614–1617. doi:10.1016/j.tetlet.2009.01.102.

[45] J.D. Moseley, P.M. Murray, E.R. Turp, S.N.G. Tyler, R.T. Burn, A mild robust generic protocol for the Suzuki reaction using an air stable catalyst, Tetrahedron. 68 (2012) 6010–6017. doi:10.1016/j.tet.2012.05.030.

[46] S. Kawai, T. Nakashima, Y. Kutsunugi, H. Nakagawa, H. Nakano, T. Kawai, Photochromic amorphous molecular materials based on dibenzothienylthiazole structure, J. Mater. Chem. 19 (2009) 3606. doi:10.1039/b823354c.

[47] T. Kawai, N. Fukuda, D. Gröschl, S. Kobatake, M. Irie, Refractive Index Change of Dithienylethene in Bulk Amorphous Solid Phase, Jpn. J. Appl. Phys. 38 (1999) 1194–1196.

[48] M.-S. Kim, T. Kawai, M. Irie, Synthesis of Amorphous Diarylethenes Having Diphenylethenyl Substituents., Chem. Lett. (2000) 1188–1189. doi:10.1246/cl.2000.1188.

[49] S. Kobatake, K. Uchida, E. Tsuchida, M. Irie, Single-crystalline photochromism of diarylethenes: reactivity-structure relationship., Chem. Commun. 2 (2002) 2804–5. http://www.ncbi.nlm.nih.gov/pubmed/12478755.

[50] G. Liu, Q. Tu, Q. Zhang, C. Fan, T. Yang, 1,2-Bis[5-(4-cyano-phen-yl)-2-methyl-3-thien-yl]-3,3,4,4,5,5-hexa-fluoro-cyclo-pent-1-ene: a photochromic diaryl-ethene compound., Acta Crystallogr. Sect. E. Struct. Rep. Online. 64 (2008) o938. doi:10.1107/S1600536808011653.

[51] M. Morimoto, S. Kobatake, M. Irie, Polymorphism of 1,2-Bis(2-methyl-5-p-methoxyphenyl-3-thienyl)perfluorocyclopentene and Photochromic Reactivity of the Single Crystals, Chem. - A Eur. J. 9 (2003) 621–627.

[52] C. Iwaihara, D. Kitagawa, S. Kobatake, Polymorphic crystallization and thermodynamic phase transition between the polymorphs of a photochromic diarylethene, Cryst. Growth Des. 15 (2015) 2017–2023. doi:10.1021/acs.cgd.5b00196.

[53] R.G. Snyder, H.L. Strauss, A. Ellinger, C-H Stretchlng Modes and the Structure of n-Alkyl Chains. 1. Long, Disordered Chains, J. Phys. Chem. 86 (1982) 5145–5150.

[54] R.S. Ho Lam, M. a. Rogers, Experimental validation of the modified Avrami model for non-isothermal crystallization conditions, CrystEngComm. 13 (2011) 866. doi:10.1039/c0ce00523a.

[55] X. Wang, Y. Zhang, Y. Yuan, J. Zhang, One dimensional main-chain crystallization kinetics of poly(3-octylthiophenes) investigated by infrared spectroscopy, Vib. Spectrosc. 71 (2014) 1–5. doi:10.1016/j.vibspec.2013.12.008.

[56] Z. Chen, J.N. Hay, M.J. Jenkins, The kinetics of crystallization of poly(ethylene terephthalate) measured by FTIR spectroscopy, Eur. Polym. J. 49 (2013) 1722–1730. doi:10.1016/j.eurpolymj.2013.03.020.

[57] Q. Xing, X. Zhang, X. Dong, G. Liu, D. Wang, Low-molecular weight aliphatic amides as nucleating agents for poly (L-lactic acid): Conformation variation induced crystallization enhancement, Polymer (Guildf). 53 (2012) 2306–2314. doi:10.1016/j.polymer.2012.03.034.

[58] Y.P. Koh, S.L. Simon, Crystallization and Vitrification of a Cyanurate Trimer in Nanopores, J. Phys. Chem. B. 116 (2012) 7754–7761.

[59] B.S. Kim, Y.G. Jeong, K. Shin, Influence of Surface Property on the Crystallization of Hentetracontane under Nanoscopic Cylindral Confinement, J. Phys. Chem. B. 117 (2013) 5978–5988.

[60] F.A. Celik, S. Kazanc, Crystallization analysis and determination of Avrami exponents of CuAlNi alloy by molecular dynamics simulation, Phys. B Condens. Matter. 409 (2013) 63–70. doi:10.1016/j.physb.2012.10.015.

Table of contents

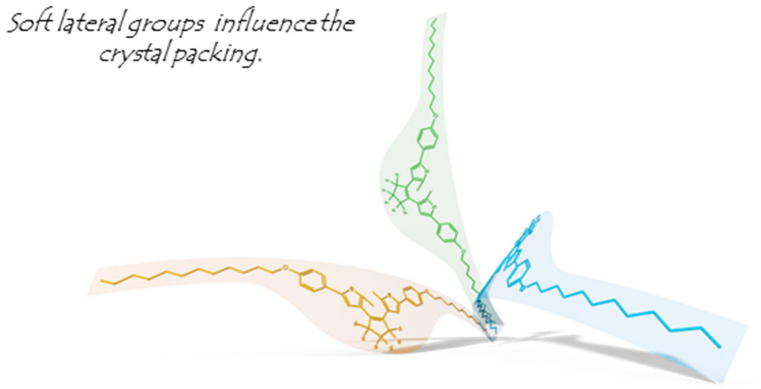

Substituents are crucial in driving the intermolecular packing arrangement in 1,2-dithienylethenes and affecting the physical properties of the solid-state materials.

Supplementary Material

The interplay of soft-hard substituents in photochromic diarylethenes

Rossella Castagna[a]*, Valentina Nardone[a,b], Giorgio Pariani[c], Emilio Parisini[b], Andrea Bianco[c]

[a] Dipartimento di Chimica Materiali e Ingegneria Chimica "G. Natta", Politecnico di Milano, piazza Leonardo da Vinci 32, 20133 Milano, Italy

[b] Center for Nano Science and Technology @PoliMi, Istituto Italiano di Tecnologia, Via Pascoli 70/3, 20133 Milano, Italy

[c] Istituto Nazionale di Astrofisica, Osservatorio Astronomico di Brera, via E. Bianchi 46, 23807 Merate, Italy

Table of contents:

Synthetic procedure

All reactions were carried out under a dry, oxygen-free argon atmosphere. Unless otherwise specified, all reagents and catalysts were commercial (Sigma Aldrich).

1,2-Bis(5-p-cyanophenyl-2-methyl-3-thienyl)perfluorocyclopentene (**DTE-1**), 1-(2-methyl-5-p-cyanophenyl-3-tienyl)-2-(2-methyl-5-p-methoxyphenyl-3-thienyl)perfluorocyclopentene (**DTE-2**) and 1,2-bis(5-p-methoxyphenyl-3-thienyl)perfluorocyclopentene (**DTE-3**)

4-Cyanophenylboronic acid (0.132 g, 1.37 mmol), **9** (0.5 g, 1.14 mmol), $Na_2CO_3 \cdot 10H_2O$ (1.31 g, 4.58 mmol), and $Pd(PPh_3)_4$ (0.132 g, 0.11 mmol) were placed in a reaction flask under inert atmosphere. DME (20 ml, degassed) and water (5 ml, degassed) were subsequently added, and the solution was refluxed under argon. After 24 hours, 4-methoxyphenylboronic acid (0.208 g, 1.37 mmol) and $Pd(PPh_3)_4$ (132 mg, 0.11 mmol) were added and heating was continued for ca. 15 hours. The mixture was quenched with water (20 ml) and ether (50 ml). The organic layer was separated and the water phase was extracted further times with ether (3 x 50 ml). The combined organic phases were dried (Na_2SO_4), filtered, and the solvent was evaporated under reduced pressure. Yellowish solid were obtained after purification by column chromatography on silica gel (petroleum ether:dichloromethane 1:1 v/v).

DTE-1 (0.04 g, 6%)

^{1}H NMR (400 MHz, $CDCl_3$): δ 7.66 (d, 4H, ^{3}J(H,H) = 8.2 Hz), 7.61 (d, 4H, ^{3}J(H,H) = 8.2 Hz), 7.37 (s, 2H), 2.01 (s, 6H) ppm. ESI-MS: m/z calcd for $C_{29}H_{16}F_6N_2S_2 + Na^+$, 593.6 [$M^+$ Na^+]; found, 593.5 (M^+).

DTE-2 (0.25 g, 38%)

^{1}H NMR (400 MHz, $CDCl_3$): δ 7.65 (d, 2H, ^{3}J(H,H) = 8.2 Hz), 7.60 (d, 2H ^{3}J(H,H) = 8.2 Hz), 7.44 (d, 2H, $^{3'}$J(H,H) = 8.2 Hz), 7.37 (s, 1H), 7.12 (s, 1H), 6.91 (d, 2H, $^{3'}$J(H,H) = 8.2 Hz), 3.83 (s, 3H), 2.02 (s, 3H), 1.96 (s, 3H) ppm. ESI-MS: m/z calcd for $C_{29}H_{19}F_6NOS_2$, 575.6 [M]; found, 575.5 (M).

DTE-3 (0.18 g, 27%)

^{1}H NMR (400 MHz, $CDCl_3$): δ 7.45 (d, 4H, ^{3}J(H,H) = 8.2 Hz), 7.14 (s, 2H), 6.90 (d, 4H, ^{3}J(H,H) = 8.2 Hz), 3.83 (s, 6H), 1.96 (s, 6H) ppm. ESI-MS: m/z calcd for $C_{29}H_{22}F_6O_2S_2$, 580.6 [M]; found, 580.5 (M).

1-Bromo-4-dodecyloxybenzene (**11**)

Following the procedure reported in a previous paper[1], 4-bromophenol **10** (10.0 g, 57.8 mmol), NaOH (2.9 g, 75.1 mmol) and 1-bromododecane (13.7 ml, 56.6 mmol) were added to 46 ml of DMSO. The reaction mixture was stirred at 100°C for 24 hours, cooled and extracted with diethyl ether. The combined layers were washed with water, dried over Na_2SO_4, filtered and the solvent removed under reduced pressure. After recrystallization from ethanol a solid was obtained in the form of white flakes (18.5 g, 94%).

^{1}H NMR (400 MHz, $CDCl_3$): δ 7.350 (d, 2H, ^{3}J(H,H)=9.0 Hz), 6.78 (d, 2H, ^{3}J(H,H)=9.0 Hz), 3.918 (t, 2H, ^{3}J(H,H)=6.6 Hz), 1.767 (m, 2H), 1.44 (m, 2H), 1.27 (b, 16H), 0.89 (t, 3H, ^{3}J(H,H)= 6.8 Hz) ppm.

4-dodecyloxybenzene boronic acid (**12**)

n-Butyllithium (2.5 M in hexane, 7.1 ml, 17.6 mmol) was added to dry THF (100 ml) cooled at -78°C. To this solution under stirring, a solution of **11** (6.0 g, 17.6 mmol) in 75 ml of dry THF was added dropwise. After 40 minutes of stirring at -78°C, trimethylborate (3.7 g, 35.2 mmol) was added and the reaction mixture was stirred for further 30 minutes at the same temperature. After warming up, the reaction was poured into an aqueous solution of HCl 37% (7 ml hydrochloric acid in 230 ml water) and stirred for 1.5 hours. The organic layer was then extracted with diethyl ether and the solvent removed under reduced pressure. The crude product was washed with methanol and filtered. The collected filtrate was dried under reduced pressure to obtain the desired product as a white solid (2.9 g, 54%).

^{1}H NMR (400 MHz, $CDCl_3$): δ 8.15 (d, 2H, ^{3}J(H,H)=8.6 Hz), 6.99 (d, 2H, ^{3}J(H,H)=8.6 Hz), 4.05 (t, 2H, ^{3}J(H,H)=6.6 Hz), 1.82 (m, 2H), 1.47 (m, 2H), 1.28 (b, 16H), 0.89 (t, 3H, ^{3}J(H,H)= 6.7 Hz) ppm.

1-(2-methyl-5-p-cyanophenyl-3-thienyl)-2-(2-methyl-5-p-dodecyloxyphenyl-3-thienyl) perfluorocyclopentene (**DTE-5**)

A solution of **9** (0.65 g, 1.49 mmol), 4-cyanophenylboronic acid pinacol ester (0.45 g, 1.96 mmol), **12** (0.540 g, 1.76 mmol), K_2CO_3 (2.6 g, 18.8 mmol),aqueous solution (13 ml) and $PdCl_2$ (dtbpf) (1,1 bis(di-tert-butylphosphino)ferrocene palladium dichloride) (0.108 g, 0.16 mmol) in previously degassed DME (13 ml) were thoroughly mixed in a process vial. The vial was capped, the mixture was heated under microwave irradiation conditions at 140 °C and 150 W for 40 minutes, and then the process vial was allowed to cool to room temperature. The reaction mixture was extracted with diethyl ether, the organic fraction were combined together, dried over Na_2SO_4, filtered, and then the solvent was removed under reduced pressure. The raw product was purified using flash

chromatography (silica gel, petroleum ether:dichloromethane 8:2 v/v) to afford 0.34 g (26 % yield) of **DTE-5** as white solid.

^{1}H NMR (400 MHz, $CDCl_3$): δ 7.66 (d, 2H, ^{3}J(H,H)= 8.4 Hz), 7.61 (d, 2H, ^{3}J(H,H)= 8.4 Hz) 7.43 (d, 2H, ^{3}J(H,H)= 8.8 Hz), 7.37 (s, 1H), 7.12 (s, 1H), 6.90 (d, 2H, ^{3}J(H,H)= 8.8 Hz), 3.98 (t, 2H, ^{3}J(H,H)= 6.5 Hz), 2.03 (s,3H), 1.97 (s, 3H), 1.79 (m, 2H), 1.46 (m, 2H), 1.27 (s, 16H), 0.89 (t, 3H, ^{3}J(H,H)= 6.8 Hz) ppm. ESI-MS: m/z calcd for $C_{40}H_{41}F_6NOS_2$, 729.8 [M]; found, 729.7 (M).

After flash chromatography also **DTE-1** (32% yield) and **DTE-7** (28% yield) were obtained.

1-(2-methyl-5-p-carboxyphenyl-3-tienyl)-2-(2-methyl-5-p-dodecyloxyphenyl-3-thienyl)perfluorocyclopentene (**DTE-4**) and 1,2-bis-(5-p-dodecyloxyphenyl-3-thienyl)perfluoro-cyclopentene (**DTE-7**)

4-Carboxyphenylboronic acid (0.125 g, 0.755 mmol), **9** (0.3 g, 0.686 mmol), **12** (0.230 g, 0.755 mmol), $Na_2CO_3 \cdot 10$ H_2O (0.785 g, 2.74 mmol), and $Pd(PPh_3)_4$ (0.08 g, 0.068 mmol) were placed in a reaction flask under inert atmosphere. DME (20 ml, degassed) and water (10 ml, degassed) were subsequently added, and the solution was refluxed under argon. After 24 hours, the mixture was quenched with water (20 ml) and ether (50 ml). The organic layer was separated, and the water phase was extracted further times with ether (3 x 50 ml). The combined organic phases were dried (Na_2SO_4), filtered, and the solvent was evaporated at reduced pressure. White-yellowish solids were obtained after purification by flash chromatography on silica gel using diethyl ether as eluent.

DTE-4 (0.11 g, 22%)

^{1}H NMR (400 MHz, $CDCl_3$): δ 8.10 (d, 2H, ^{3}J(H,H) = 8.1 Hz), 7.62 (d, 2H, ^{3}J(H,H) = 8.1 Hz), 7.44 (d, 2H, ^{3}J(H,H) = 8.8 Hz), 7.40 (s, 1H), 7.14 (s, 1H), 6.89 (d, 2H, ^{3}J(H,H) = 8.8 Hz), 3.98 (t, 2H, ^{3}J(H,H) = 6.5 Hz), 2.00 (s, 3H), 1.96 (s, 3H), 1.78 (m, 2H), 1.46 (m, 2H), 1.27 (m, 16H), 0.88 (t, 3H, ^{3}J(H,H) = 6.8 Hz) ppm. ESI-MS: m/z calcd for $C_{40}H_{42}F_6O_3S_2$ - H^+, 748.8 [M - H^+]; found, 747.7 (M – H^+).

DTE-7 (0.06 g, 10%)

^{1}H NMR (400 MHz, $CDCl_3$): δ 7.44 (d, 4H, ^{3}J(H,H) = 8.7 Hz), 7.14 (s, 2H), 6.89 (s, 4H, ^{3}J(H,H) = 8.7 Hz), 3.98 (t, 4H, ^{3}J(H,H) = 6.4 Hz), 1.96 (s, 6H), 1.79 (m, 4H), 1.46 (m, 4H), 1.28 (b, 32H), 0.89 (t, 6H, ^{3}J(H,H) = 6.8 Hz) ppm. ESI-MS: m/z calcd for $C_{51}H_{66}F_6O_2S_2$, 889.1 [M]; found, 889.0 (M).

1,2-Bis-(5-p-hydroxyphenyl-2-methyl-3-thienyl)perfluorocyclopentene (**8**)

In a reaction flask containing compound **DTE-3** (0.5 g, 0.86 mmol) acetic acid (30 ml), hydrobromic acid (48% wt. in water, 12 ml) and acetic anhydride (5 ml) were added. The reaction mixture was than refluxed for 8 hours in the dark. The mixture was washed several times with a saturated solution of $NaHCO_3$, extracted with diethyl ether and dried over Na_2SO_4. After solvent removal, a greyish powder of compound **8** was obtained in quantitative yield.

^{1}H NMR (400 MHz, $CDCl_3$): δ 7.41 (d, 4H, ^{3}J(H,H) = 8.6 Hz), 7.13 (s, 2H), 6.84 (d, 4H, ^{3}J(H,H) = 8.6 Hz), 1.96 (s, 6H) ppm.

1,2-Bis-(5-p-hexylphenoxyphenyl-3-thienyl)perfluorocyclopentene (**DTE-6**)

In a reaction flask containing **8** (0.250 g, 0.452 mmol), K_2CO_3 (0.188 g, 1.36 mmol) in 15 ml acetonitrile and 1-bromohexane (0.190 ml, 1.36 mmol) was added and refluxed for 24 hours. After 24 hours, the completeness of the reaction was confirmed by TLC. The mixture was extracted with diethyl ether and dried over Na_2SO_4. The crude was washed with ethanol and the desired product was obtained as a white solid (0.29 g) with a 90% yield.

^{1}H NMR (400 MHz, $CDCl_3$): δ 7.44 (d, 4H, ^{3}J(H,H) = 8.6 Hz), 7.14 (s, 2H), 6.90 (d, 4H, ^{3}J(H,H) = 8.6 Hz), 3.98 (t, 4H, ^{3}J(H,H) = 6.5 Hz), 1.96 (s, 6H), 1.79 (m, 4H), 1.47 (m, 4H), 1.36 (m, 8H), 0.92 (t, 6H, ^{3}J(H,H) = 6.9 Hz) ppm. ESI-MS: m/z calcd for $C_{39}H_{42}F_6O_2S_2$, 720.9 [M^+]; found, 720.8 (M).

[1] J.E. Klare, G.S. Tulevski, K. Sugo, A. De Picciotto, K. a White, C. Nuckolls, Cruciform pi-systems for molecular electronics applications., J. Am. Chem. Soc. 125 (2003) 6030–1. doi:10.1021/ja0350942.

DFT calculation results

The calculations have been performed using Gaussian 09 (G09RevD.01) with a basis set 6-31G(p,d) and B3LYP as functional.

Figure S1. Equilibrium geometry with the corresponding Energy for the open and closed form

Open form

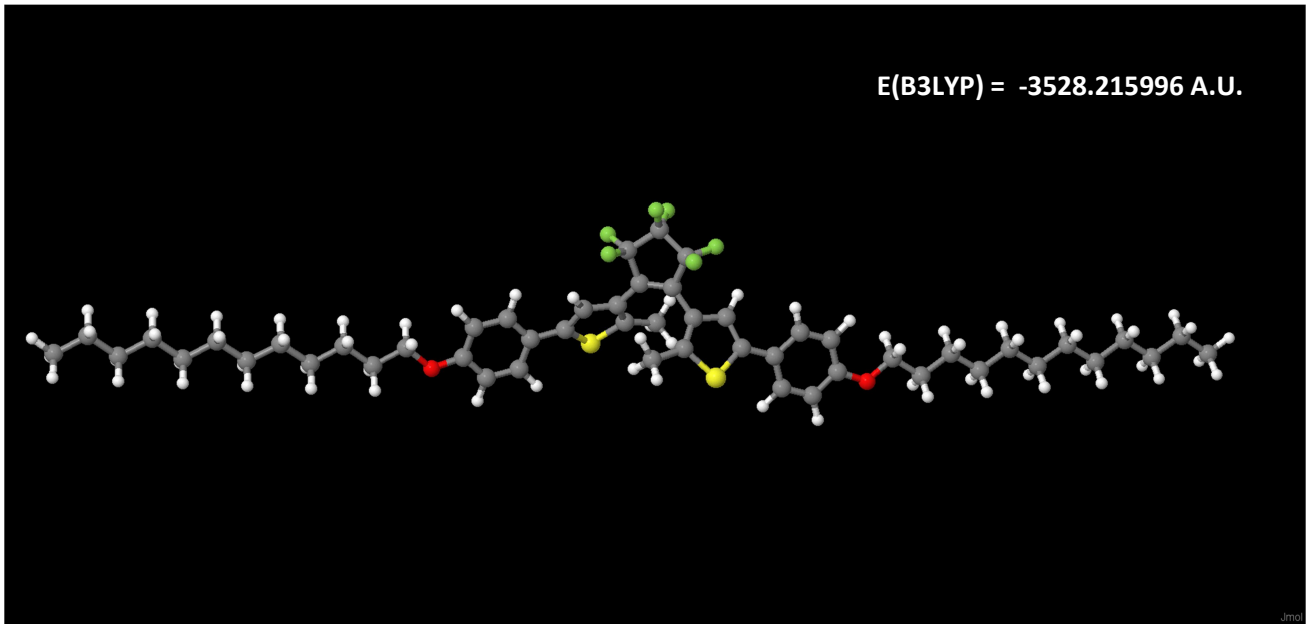

Dipole moment (μ_x, μ_y, μ_z): 2.32561468E-02, -9.67489818E-01, -3.84852441E-02 a.u.

Electronic Polarizability (α_{xx}, α_{xy}, α_{yy}, α_{xz}, α_{yz}, α_{zz}): 1.04088415E+03, 1.28897627E-01, 5.30820166E+02, -5.80822380E+00, -1.11964652E+01, 4.02383127E+02 a.u.

Closed form

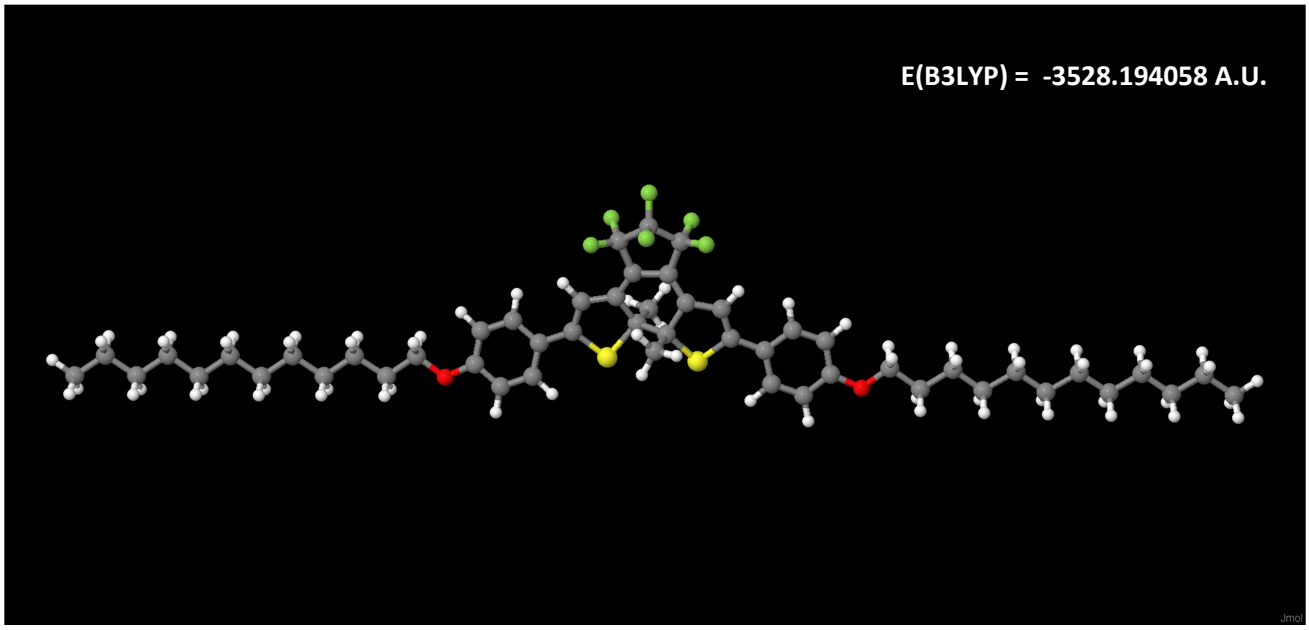

Dipole moment (μ_x, μ_y, μ_z): -1.83186862E-02, -1.39452123E+00, -6.07606633E-02 a.u.

Electronic Polarizability (α_{xx}, α_{xy}, α_{yy}, α_{xz}, α_{yz}, α_{zz}): 1.32321804E+03, 6.69408171E+00, 5.87563908E+02, 2.84717324E+01, -2.82910430E+01, 3.79221567E+02 a.u.

Figure S2. Infrared spectra (the frequency are scaled with a factor 0.967 and the intensities are normalized). The scaling of the calculated vibrational frequencies is a common procedure and the valued depends on many factors (among which the basis set and the functional)[2]

Open form

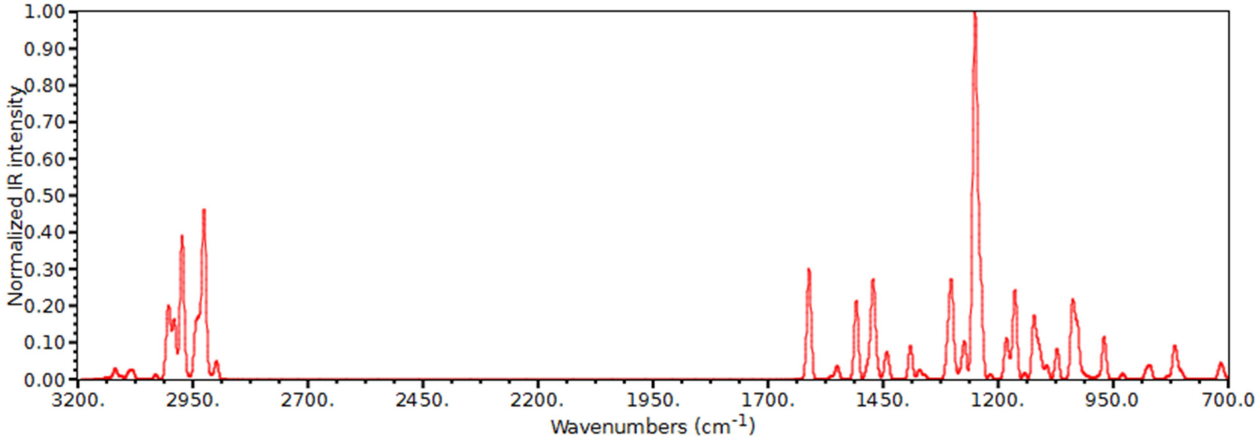

Closed form

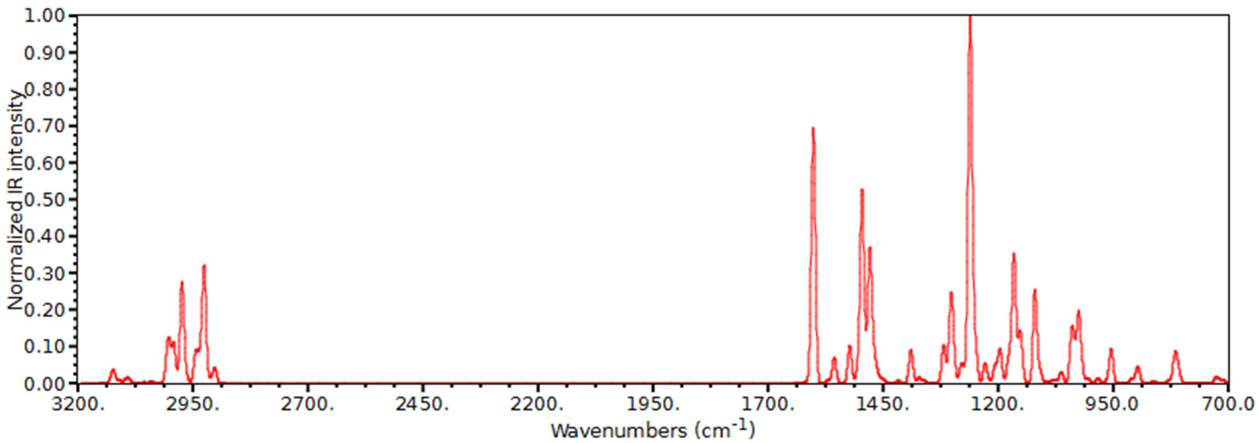

[2] G. Rauhut, P. Pulay, Transferable Scaling Factors for Density Functional Derived Vibrational Force Fields, J. Phys. Chem. 99 (1995) 3093-3100

Crystallographic Data

DTE-2: Single colourless crystals were grown by slow evaporation from a hexane:dichloromethane solution (1:1 *v/v*) of **DTE-2** at room temperature. X-ray diffraction data were collected at 100K on a crystal of size 0.14 x 0.11 x 0.07 mm using CuKα radiation. Crystal data: $C_{29}H_{19}ONS_2F_6$ M_r=575.57 Da; monoclinic, $P2_1/c$; a=25.334(1)Å, b=9.3039(5)Å, c=10.7118(6)Å; α= γ=90.00°; γ=90.484(2)°; Z=4; V=2524.7(2)Å^3; μ=2.539 mm^{-1}. A total of 355 parameters were used. All non-hydrogen atoms were refined anisotropically. The structure was refined by full matrix least-squares refinement (on F^2) and converged to a final R value of 0.029 [wR(F^2)= 0.080, S=1.009 for 4546 reflections with I > 2σ(I)]. The final difference map was featureless ($\Delta_{\rho max}$= 0.40 eÅ^{-3}, $\Delta_{\rho min}$= -0.27 eÅ^{-3})

DTE-4: Single colourless crystals were grown by vapour diffusion of ethanol in a benzene solution of **DTE-4** at 4°C. X-ray diffraction data were collected at 100K on a crystal of size 0.16 x 0.12 x 0.08 mm using CuKα radiation. Crystal data: $C_{40}H_{42}O_3S_2F_6$ M_r=748.86 Da; triclinic, P-1; a=10.012(1)Å, b=13.376(1)Å, c=14.083(1)Å; α=82.139(6)°, β=84.129(6)°, γ=80.454(6)°; Z=2; V=1836.2(3)Å^3; μ=1.902 mm^{-1}. A total of 481 parameters were used. All non-hydrogen atoms were refined anisotropically. The structure was refined by full matrix least-squares refinement (on F^2) and converged to a final R value of 0.041 [wR(F^2)= 0.122, S=1.072 for 5502 reflections with I > 2σ(I)]. The final difference map was featureless ($\Delta_{\rho max}$= 0.36 eÅ^{-3}, $\Delta_{\rho min}$ = -0.28 eÅ^{-3})

DTE-5: Single colourless crystals were grown by slow evaporation of a hexane:ethyl acetate solution (1:1 *v/v*) of **DTE-5** at room temperature. A crystal of size 0.17 x 0.13 x 0.09 mm was selected for the determination of cell parameters and data collection at 100K using CuKα radiation. Crystal data: $C_{40}H_{41}OS_2F_6N$ M_r=729.86 Da; monoclinic, $P2_1/c$; a=35.511(4)Å, b=9.369(1)Å, c=10.754(1)Å; α=γ=90°, β=92.122(5)°; Z=4; V=3575.5(7)Å^3; μ=1.905 mm^{-1}. A total of 469 parameters were used. All non-hydrogen atoms were refined anisotropically. The structure was refined by full matrix least-squares refinement (on F^2) and converged to a final R value of 0.044 [wR(F^2)= 0.127, S=1.030 for 5477 reflections with I > 2σ(I)]. The final difference map was featureless ($\Delta_{\rho max}$= 0.82 eÅ^{-3}, $\Delta_{\rho min}$= -0.63 eÅ^{-3})

DTE-6: Single colourless crystals were grown by slow evaporation of a dichloromethane solution of **DTE-6** at room temperature. X-ray diffraction data were collected at 100K from a crystal of size 0.20 x 0.15 x 0.10 mm using CuKα radiation. Crystal data: $C_{19.50}H_{21}OSF_3$ M_r=360.42 Da; monoclinic, C2/c; a=35.223(3)Å, b=9.4116(7)Å, c=10.5398(7)Å; α= γ=90.00°; β=96.642(5)°; Z=8; V=3470.5(5)Å^3; μ=1.967 mm^{-1}. A total of 231 parameters were used. All non-hydrogen atoms were refined anisotropically. The structure was refined by full matrix least-squares refinement (on F^2) and converged to a final R value of 0.112 [wR(F^2)= 0.340, S=1.086 for 2299 reflections with I > 2σ(I)]. The final difference map was featureless ($\Delta_{\rho max}$= 1.33 eÅ^{-3}, $\Delta_{\rho min}$= -0.96 eÅ^{-3})

DTE-7: Single colourless crystals were grown by slow evaporation of a pyridine solution of **DTE-7** at 4°C. X-ray diffraction data were collected at 100K on a crystal of size 0.08 x 0.06 x 0.05 mm using CuKα radiation. Crystal data: $C_{51}H_{66}O_2S_2F_6$ M_r=889.16 Da; triclinic, P-1; a=6.3963(6)Å, b=15.894(1)Å, c=24.779(2)Å; α=101.148(6)° β=96.472(6)°; γ=98.311(6)°, Z=2; V=2419.5(4)Å^3; μ=1.501 mm^{-1}. A total of 570 parameters were used. All non-hydrogen atoms were refined anisotropically. The structure was refined by full matrix least-squares refinement (on F^2) and converged to a final R value of 0.119 [wR(F^2)= 0.327, S=1.282 for 3755 reflections with I > 2σ(I)]. The final difference map was featureless ($\Delta_{\rho max}$= 0.55 eÅ^{-3}, $\Delta_{\rho min}$= -0.56 eÅ^{-3})

Structural disorder was observed in **DTE-6**, for which two alternative conformations of the alkoxy chains could be modelled and assigned a 0.7 and 0.3 occupancy factor, respectively (Fig. S3).

Table S1: Crystal data

Crystal data	DTE-2	DTE-4	DTE-5	DTE-6	DTE-7
Chemical formula	$C_{29}H_{19}ONS_2F_6$	$C_{40}H_{42}O_3S_2F_6$	$C_{40}H_{41}OS_2F_6N$	$C_{19.50}H_{21}OSF_3$	$C_{51}H_{66}O_2S_2F_6$
M_r (Da)	575.57	748.86	729.86	360.42	889.16
Crystal system, space group	Monoclinic, $P2_1/c$	Triclinic, P-1	Monoclinic, $P2_1/c$	Monoclinic, C2/c	Triclinic, P-1
Temperature (K)	100	100	100	100	100
a, b, c (Å)	25.334(1), 9.3039(5), 10.7118(6)	10.012(1), 13.376(1), 14.083(1)	35.511(4), 9.369(1), 10.754(1)	35.223(3), 9.4116(7), 10.5398(7)	6.3963(6), 15.894(1), 24.779(2)
α, β, γ	90.00, 90.484(2), 90.00	82.139(6), 84.129(6), 80.454(6)	90.00, 92.122(5), 90.00	90.00, 96.642(5), 90.00	101.148(6), 96.472(6), 98.311(6)
V ($Å^3$)	2524.7(2)	1836.2(3)	3575.5(7)	3470.5(5)	2419.5(4)
Z	4	2	4	8	2
Radiation type	CuKα	CuKα	CuKα	CuKα	CuKα
μ (mm^{-1})	2.539	1.902	1.905	1.967	1.501
Crystal size (mm)	0.14 x 0.11 x 0.07	0.16 x 0.12 x 0.08	0.17 x 0.13 x 0.09	0.20 x 0.15 x 0.10	0.08 x 0.06 x 0.05
Absorption correction	Multi-scan	Multi-scan	Multi-scan	Multi-scan	Multi-scan
Theta range for data collection (°)	1.74 to 69.23	3.18 to 68.83	3.74 to 66.60	4.87 to 68.87	2.88 to 69.12
No. of measured, unique and unique with [I > 2σ(I)] reflections	36302, 4668, 4546	19978, 6619, 5502	38363, 6047, 5477	14969, 3126, 2299	21260, 8453, 3756
R_{int}	0.0278	0.0461	0.0389	0.0457	0.1073
Limiting indices	-28<=h<=30, -11<=k<=10, -9<=l<=12	-12<=h<=10, -16<=k<=16, -16<=l<=16	-42<=h<=42, -10<=k<=11, -12<=l<=8	-33<=h<=42, -10<=k<=11, -12<=l<=8	-5<=h<=7, -19<=k<=17, -29<=l<=29
$R[F^2 > 2\sigma(F^2)]$, $wR(F^2)$, S	0.029, 0.080, 1.009	0.041, 0.122, 1.072	0.044, 0.127, 1.030	0.112, 0.340, 1.086	0.119, 0.327, 1.277
No. of param./restraints	355/0	481/0	469/2	231/211	570/1
H-atom treatment	Mixed	Mixed	Mixed	Mixed	Mixed

Δ_{pmax} Δ_{pmin} (e Å^{-3})	0.40, -0.27	0.36, -0.28	0.82, -0.63	1.33, -0.96	0.55, -0.56

Table S2: Distance between active carbon (Å) (red dotted line) and torsional angles (°) thiophene-phenyl rings; for clarity, the aryl groups are identified in each molecule by their substituents (R and R').

	DTE-1	DTE-2	DTE-3	DTE-4	DTE-5	DTE-6	DTE-7
C-C	3.601	3.495	3.523	3.540	3.490	3.555	3.637
R	21.89	-18.08	22.87	25.05	-17.29	-14.88	2.31
R'	21.89	20.22	-25.04	18.44	20.04	-14.88	32.47

*polymorph γ (CSD #185944)

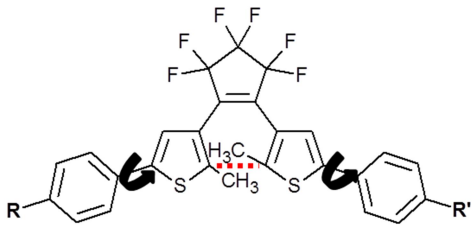

DTE-1 R = CN R' = CN

DTE-2 R = CN R' = OMe

DTE-3 R = OMe R' = OMe

DTE-4 R = COOH R' = $OC_{12}H_{25}$

DTE-5 R = CN R' = $OC_{12}H_{25}$

DTE-6 R = OC_6H_{13} R' = OC_6H_{13}

DTE-7 R = $OC_{12}H_{25}$ R' = $OC_{12}H_{25}$

Figure S3. ORTEP representation of the molecular structures for the five novel DTE structures reported in this work.

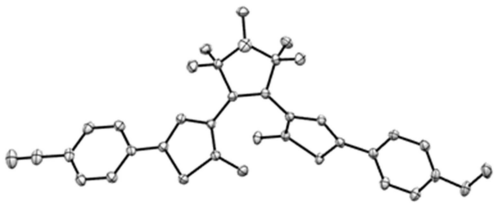

DTE-2

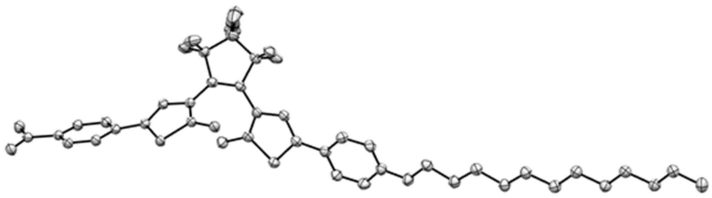

DTE-4

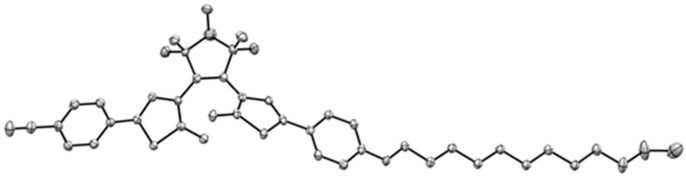

DTE-5

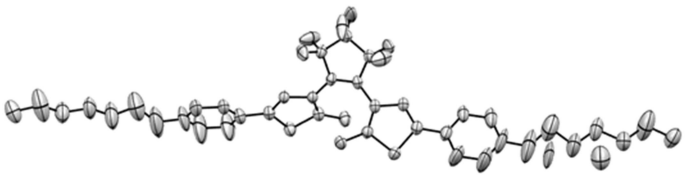

DTE-6

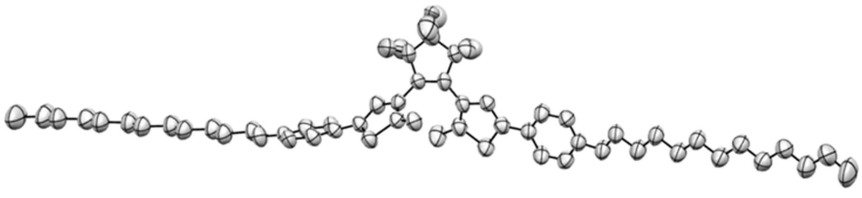

DTE-7

Figure S4. The crystal packing of DTE-5 and DTE-7 showing the interdigitation of the C12 chains.

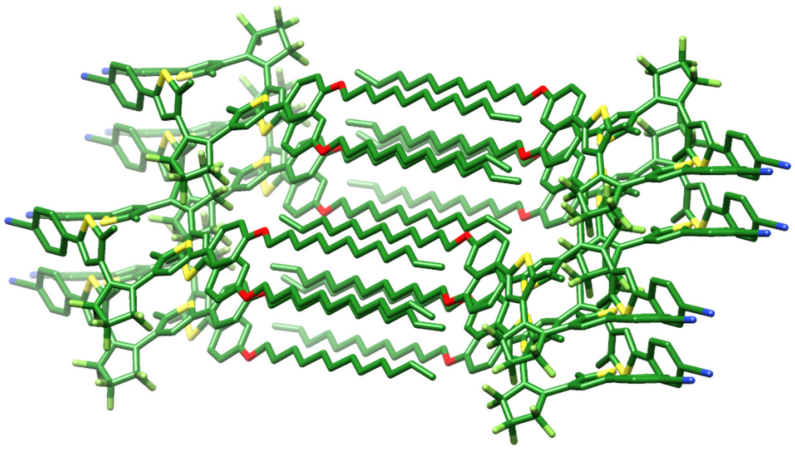

DTE-5

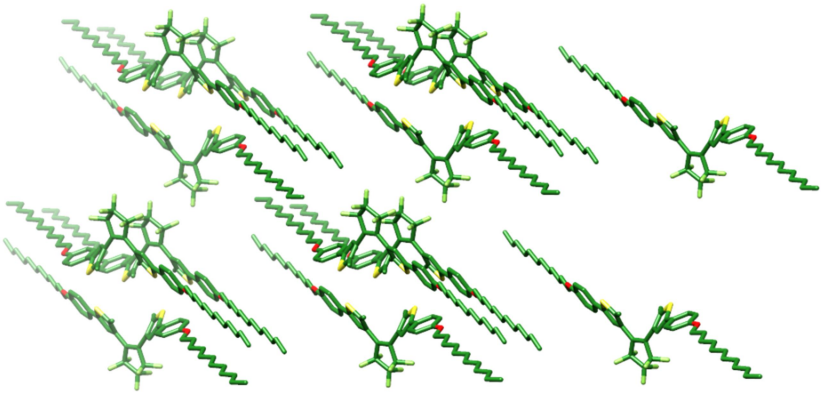

DTE-7

Figure S5. UV- vis spectra of different DTEs thin films of pure compound deposited onto quartz. The spectra of the closed form is reported at the photostationary state conversion (PPS), obtained by illuminating the sample at the absorption peak of the open form. Dotted line means that in the UV region below the 400 nm scattering phenomena can affect the spectra.

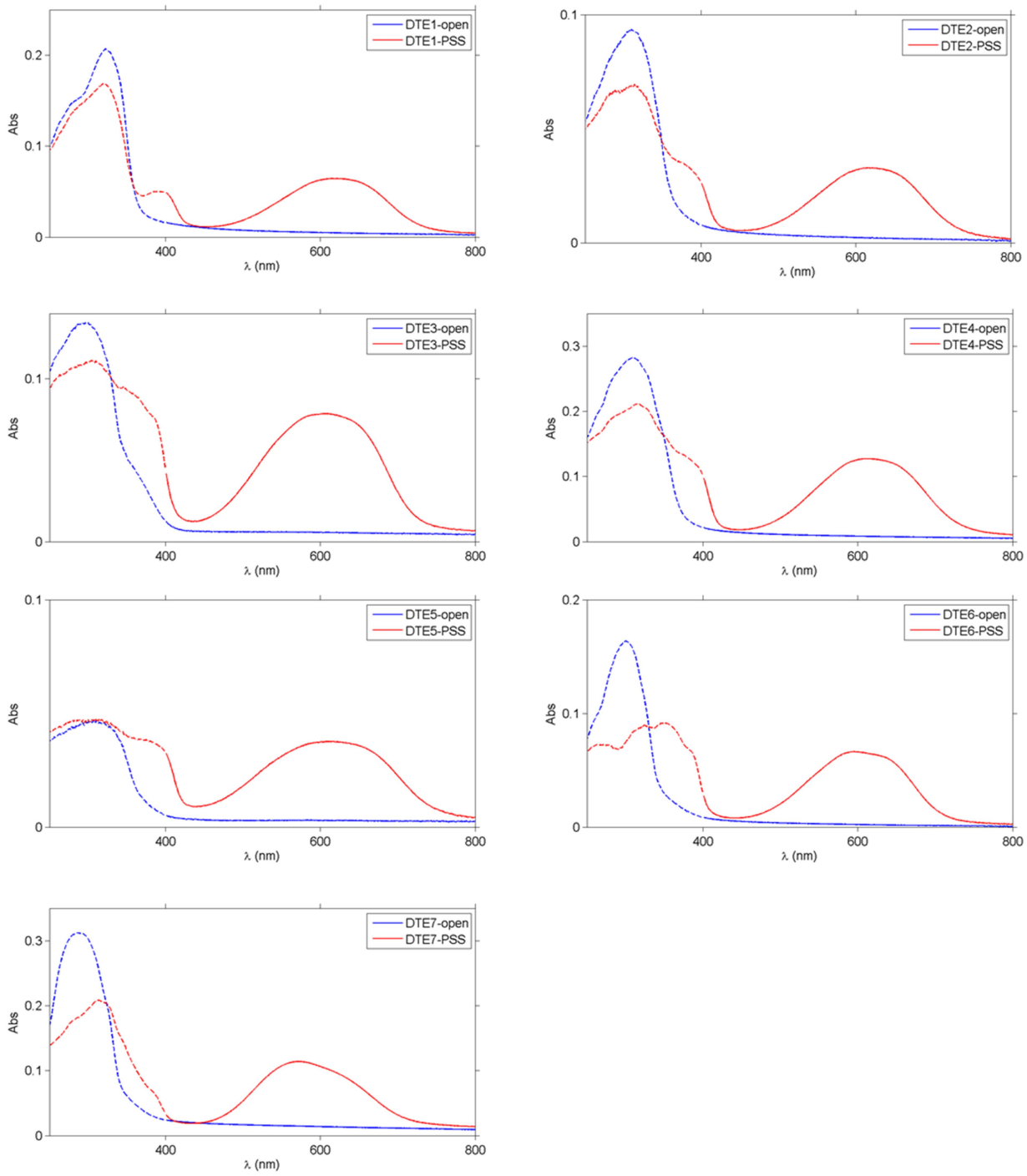

Table S3 - UV-visible absorption maxima and absorption coefficients of the open and the photostationary (PSS) forms of the DTEs under study in hexane solution.

	Open form		Closed form	
	λ_{OPEN} [nm]	ε (λ_{OPEN}) [1/(Mcm)]	λ_{PSS} [nm]	ε (λ_{PSS}) [1/(Mcm)]
DTE-1	315	33100	591	11400
DTE-2	306	37800	597	18100
DTE-3	293	43800	582	20000
DTE-4	307	13200	597	6250
DTE-5	305	35400	603	16600
DTE-6	297	41500	582	21000
DTE-7	295	36500	582	17000

Figure S6. DSC scan under nitrogen atmosphere heating 20°C /min from 0°C to 250°C, cooling at 5°C/min from 250°C to 0°C. Photochromic powder (c.a. 3.5 mg) is loaded in an aluminium pan. DTE-6 show the presence of two polymorphs as investigated by Iwaihara et. al [1]

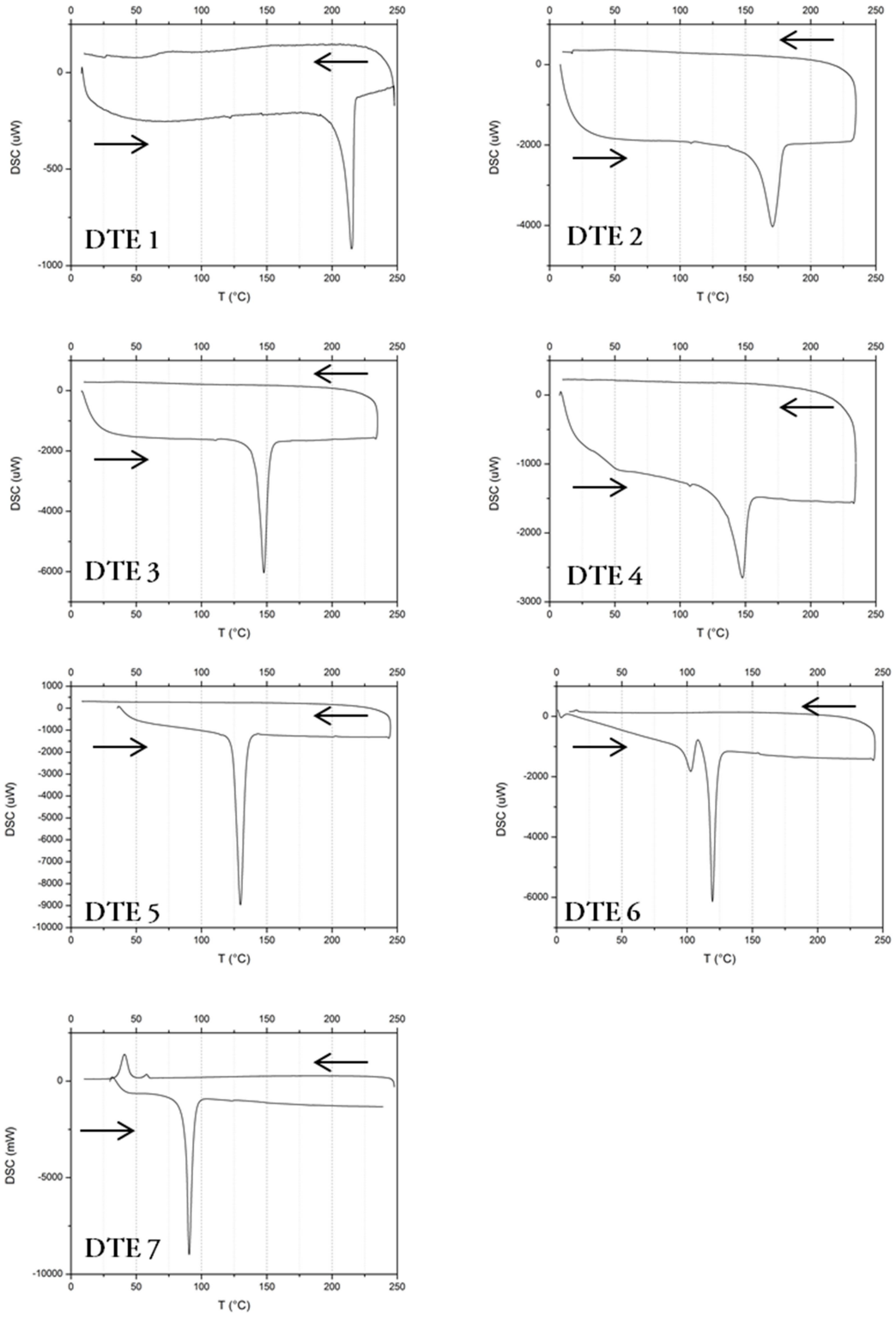

[1] C. Iwaihara, D. Kitagawa, S. Kobatake, Polymorphic Crystallization and Thermodynamic Phase Transition between the Polymorphs of a Photochromic Diarylethene, Cryst. Growth Des. 15 (2015) 2017-2023

Figure S7. Comparison of the calculated (scale factor = 0.967) and experimental IR spectra for the open form with highlighted the band that changes during the crystallization process and the corresponding normal modes involved.